# Situation-based neuromorphic memory in spiking neuron-astrocyte network

Susanna Gordleeva, Yuliya A. Tsybina, Mikhail I. Krivonosov, Ivan Y. Tyukin, Victor B. Kazantsev, Alexey A. Zaikin, Alexander N. Gorban

***Abstract*—Mammalian brains operate in a very special surrounding: to survive they have to react quickly and effectively to the pool of stimuli patterns previously recognized as danger. Many learning tasks often encountered by living organisms involve a specific set-up centered around a relatively small set of patterns presented in a particular environment. For example, at a party, people recognize friends immediately, without deep analysis, just by seeing a fragment of their clothes. This set-up with reduced "ontology" is referred to as a "situation". Situations are usually local in space and time. In this work, we propose that neuron-astrocyte networks provide a network topology that is effectively adapted to accommodate situation-based memory. In order to illustrate this, we numerically simulate and analyze a well-established model of a neuron-astrocyte network, which is subjected to stimuli conforming to the situation-driven environment. Three pools of stimuli patterns are considered: external patterns, patterns from the situation associative pool regularly presented to the network and learned by the network, and patterns already learned and remembered by astrocytes. Patterns from the external world are added to and removed from the associative pool. Then we show that astrocytes are structurally necessary for an effective function in such a learning and testing set-up. To demonstrate this we present a novel neuromorphic computational model for short-term memory implemented by a two-net spiking neural-astrocytic network. Our results show that such a system tested on synthesized data with selective astrocyte-induced modulation of neuronal activity provides an enhancement of retrieval quality in comparison to standard spiking neural networks trained via Hebbian plasticity only. We argue that the proposed set-up may offer a new way to analyze, model, and understand neuromorphic artificial intelligence systems.**

***Index Terms*—Spiking neural network, astrocyte, neuron-astrocyte interaction, working memory.**

## I. Introduction

THE way the test data is organized, validated, as well as the method used to train learning systems can critically affect the result. Especially if the quality of learning is directly linked to survival. Mammalian brains are trained to survive, which is why they enable an animal to react quickly to patterns previously associated with dangerous situations. Hence, it is important to understand how such quick responses emerge in highly uncertain and complicated real-world operational conditions.

The cornerstone assumption of the classical statistical learning frameworks [1], [2], [3] is that a learner or a learning machine operates in an environment which can be adequately modelled by some unknown probability distribution. The learner then gathers relevant information about the environment by accessing independent samples from this unknown distribution. The problem, however, is that these apparently sensible classical assumptions have major consequences affecting the applicability of the theory. The independence assumption may be violated when the learner's training data inherits strong temporal correlations (e.g. subsequent frames taken from video footage) and which have been ignored at the data-processing stage. The absence of any knowledge about the fixed probability distribution, which is particularly difficult to alleviate in high-dimensional settings, enforces conservative worst-case distribution-agnostic generalisation bounds [1], [2], [3] and can lead to a stream of foundational paradoxes highlighting the potential impossibility to compute stable and accurate learning machines [4][1]. Finally, the fact that the distribution is fixed and unknown has an impact on the possibility to handle concept drifts – a widespread phenomenon in real-life practical applications [5]. We suggest that the above difficulties can potentially be overcome via the introduction of a new mode of learning which we will refer to as *situation-based learning*.

How many people did you meet yesterday? 5? 10? Was it difficult to recognise them? Psychologists say that our day-to-day activities impact our behaviour. Recognition of patterns around us occurs in, what is called in psychology, a situation. Obviously, biological creatures that require less time to recognise a situation are getting an evolutionary advantage, they can escape a predator faster, get a higher chance of catching a prey, or when humans are concerned, earn more

Manuscript received ; revised (Corresponding authors: Alexey Zaikin, Susanna Gordleeva.)

Susanna Gordleeva, Yuliya A. Tsybina, Mikhail Krivonosov and Victor Kazantsev are with the Lobachevsky State University of Nizhny Novgorod, Nizhny Novgorod, Russia (e-mail: gordleeva@neuro.nnov.ru, lotarevaj@gmail.com, mike_live@mail.ru, kazantsev@neuro.nnov.ru).

Susanna Gordleeva and Victor Kazantsev are with the Laboratory of Neurobiomorphic Technologies, The Moscow Institute of Physics and Technology, Moscow, Russia

Yuliya A. Tsybina and Alexey Zaikin are with the Centre for analysis of complex systems, Sechenov First State Medical University, Moscow, Russia

Ivan Tyukin is with the King's College London, UK (e-mail: ivan.tyukin@kcl.ac.uk)

Alexander Gorban is with University of Leicester, Leicester, UK (e-mail: a.n.gorban@leicester.ac.uk).

Alexey Zaikin is with Institute for Women's Health and Department of Mathematics, University College London, London, UK (e-mail: alexey.zaikin@ucl.ac.uk).

[1]See also Theorem 7.1 from [1] showing that an arbitrarily small perturbation added to an activation function has the capacity to make the Vapnik-Chervonenkis dimension of a neuron with this modified activation function infinite and hence rendering all classical generalisation bounds using Vapnik-Chervonenkis dimension useless for neural networks with such neurons.

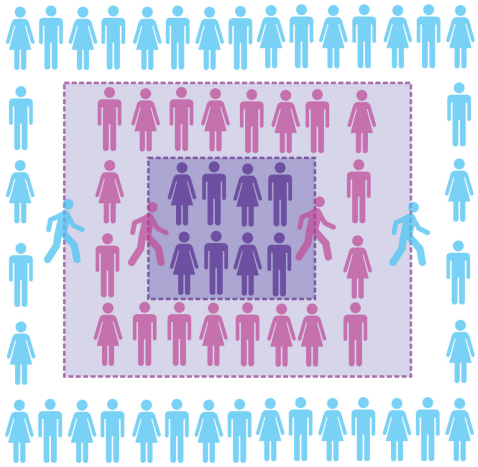

Fig. 1. A diagram of situation-based model of data. In this model, all data are partitioned into three pools of patterns. The largest circle of patterns (light blue) is the external world that contains a huge number of patterns. Situation-based pool of patterns is much smaller and includes only the patterns that we meet regularly within this situation (purple). Data patterns in the situation-based pool can be removed and replaced with patterns from the external world. Patterns from this pool are used for learning much more often than a random pattern from the external world pool, hence many of them are already learned, stored, and can be easily and quickly recognised by association with patterns stored in the system (dark blue lila).

money. We all live in a situation-ridden world, and our life is based on recognition of patterns in current situation. But how is this recognition organized? We do not normally spend much time to recognize a friend, a fraction of a pattern is usually enough. Such quick processing of is provided by a very special structure of pattern learning. We learn patterns from a situation-based pool, and, since the number of patterns in the situation is limited, our pool usually is much smaller than in the whole external world. Such a situation-based structure of learning is visualised in the Fig. 1. There are three pools of patterns. Patterns from the huge external pool get into a situation-based pool, and then they become available for learning much more often than the ones arriving directly from the external pool. Hence, all patterns from a situation pool, except for the newcomers, are learnt and stored in the memory - the internal pool. Recognition is, hence, structure-associated, and patterns from the structure pool are recognised much easier and quicker patterns than from an external pool.

Obviously, such situation-based structure has two main advantages: it is quick and requires less energy, which is very important in the biological world. Creatures adapted to such structure-oriented pattern of learning are more competitive and have an evolutionary advantage. This new data model is complementary to other important characteristics of learning and memory explored in the previous work, including high-dimensionality of the space of stimuli [6], [7] and properties of data distributions conforming to the task of learning from few examples [8], [9]. The importance of the problem was mentioned by [10], [11]. The notion of the situation captures spatiotemporal localisation of the task and the subjectivity of learners, i.e. the relevant contexts. This enables a learner to partition the complexity of the environment into the union of much simple "sparse" tasks. A related notion of *attention* in deep learning has already been proven successful in the area of natural language processing giving rise to the popular *transformer* models [12]. Here we formalise the notion at the conceptual level regardless of its particular implementation in a learning machine.

All this leads to the key question whether there exists a structural organisation of neural circuitry that is particularly suited for structure-based learning and that possesses characteristics of information processing in these circuits that are necessary to support this learning. In this paper, we propose relevant neural circuits that are particularly suited to facilitate situation-based learning. These circuits or networks combine conventional neurons and astrocytes.

The structural, metabolic, and homeostatic functions of astrocytes are well established [13]. Recently it has been revealed that astrocytes contribute to neural information processing via bidirectional exchange of regulatory signals with the neuronal elements. Astrocytes respond to neural activity by intracellular calcium elevations [14]. Calcium pulses in astrocytes induce the release of chemical transmitters (termed "gliotransmitters") which then regulate the synaptic gain of near and distant tripartite synapses at diverse timescales [15]. The data show that an astrocytes have an impact on local synaptic plasticity, neuronal network oscillations, memory and behaviour (for recent reviews see [16]–[18]). Despite that the role played by astrocytes is not yet fully understood, these recent findings support the hypothesis that *cognitive processing and memory are not the result of neuronal activity only but of the coordinated activity of both astrocytes and neurons* [19]. Consequently, the most interesting research question is: whether a presence of astrocytes, which provide multiplex topology of a recognition network with different time and spatial scales of communication, facilitates the ability of the network to work with structure-associated learning? In this paper, we investigate this question and show numerically that neuron-astrocyte networks indeed play a key role in situation-based recognition. This function is also closely linked to the idea of local corrections in large neural networks working with big data [7].

## II. Related work

Although astrocytic involvement in the information processing in the brain has been widely shown experimentally [16], there is a lack of computational studies of neural circuits focusing on astrocyte signaling in the context of learning and memory. The importance of computational modelling for developing better understanding of nature and findings answers to open questions is difficult to overestimate. Examples of works where such modelling brought new knowledge are numerous. In the area of astrocytes modelling, recent study [20] successfully demonstrated the self-repairing capability of distributed spiking neuron-astrocyte network in a robotic obstacle avoidance application. Nazari and colleages [21] studied the information transmission between the cortical spiking neural network and the cortical neuron–astrocyte network. They showed how cortical spiking network managed to improve its pattern recognition performance without the

need for retraining by receiving an additional information from neuron-astrocyte network. In addition, scholars proposed several digital implementations of astrocytic dynamics [22] and neuron-astrocyte interaction [23], [24]. In our previous works, we investigated how the astrocyte-induced dynamic coordination in the neuronal ensembles [25]–[27] induces the generation of integrated information sets [28]–[30]. Moreover, we showed that biologically-inspired spiking neuron-astrocyte network can implement the multi-item short-term memory [31]–[33]. We revealed that several information patterns can be maintained in memory at the time scale of calcium elevation in astrocytes, while the readout by the neurons due to the astrocyte-induced activity-dependent short-term synaptic plasticity resulted in local spatial synchronization in neuronal ensembles. Following our approach, a recent modeling study [34] investigated the contribution of astrocytic modulation of synaptic transmission to the formation of different modes of short-term working memory encoding. Another computational model predicts that the duration and stability of working memory representations can be altered by astrocytic signaling [35]. We further showed that spiking neuron-astrocyte network can reliably store not only binary but also analogous information patterns in short-term memory [36]. However, the work in this paper goes much further and proposes a new bio-inspired two-net spiking neuron-astrocyte network (SNAN) for more complex learning tasks, in which SNAN is implemented for associated learning.

## III. Significance

In this paper, we present three key findings: (1) a novel approach to formalizing machine learning data, namely, the temporal organization of the data as opposed to the widely accepted IID data sampling; (2) a novel neuromorphic computational model for short-term memory implemented by SNAN; and, (3) a proof, through rigorous computational experiments, that SNAN tested on synthesized data with selective astrocyte-induced modulation of neuronal activity may provide an enhancement of retrieval quality in comparison to a standard SNN trained via Hebbian plasticity. The proposed SNAN is a hybrid system, which combines the fast-spiking neural networks pre-trained by the Spike Timing Dependent Plasticity (STDP) rule with the general data set, and a slow astrocytic network, which provides time-dependent data buffering via calcium activity and gliatransmitter-induced spatial-temporal coordination of neural network activity.

## IV. Situation-based learning in spiking neuron-astrocyte network model

The concept of the proposed situation-based memory model is schematically summarized in Fig. 2. A new biologically motivated computational model of short-term memory is implemented through interaction of neural and astrocytic networks. The model acts at multiple timescales: at a millisecond scale of firing neurons and the second scale of calcium dynamics in astrocytes. The neuronal network consists of randomly sparsely connected excitatory and inhibitory spiking neurons with plastic synapses. To train synapses in neural network, we used the traditional spike-timing-dependent plasticity (STDP) rule. Astrocytes track the neural activity and respond to it by intracellular calcium elevations, which trigger the release of gliotransmitters. Gliotransmitter-induced short-term synaptic plasticity results in local spatial synchronization in neuronal ensembles. The short-term memory realized by such astrocytic modulation is characterized by one-shot learning and is maintained for seconds. The astrocytic influence on the synaptic connections during the elevation of calcium concentration implements Hebbian-like synaptic plasticity differentiating between specific and non-specific activations. Composed of two building blocks, e.g., fast-spiking neurons and slow astrocytes, the proposed memory architecture eventually demonstrated synergetic functionality in loading information. The readout of this memory by the neuronal block and storage implemented by the astrocytes.

### A. Spiking neuron-astrocyte network architecture

The architecture of the proposed SNAN is illustrated in Fig. 3. The SNAN includes three interacting layers: the layer of pyramidal neurons, the layer of interneurons, and the astrocytic layer. An input signal encoded as two-dimensional patterns was applied to the first layer. The first layer consists of 6241 ($79 \times 79$) synaptically coupled pyramidal neurons, which are connected randomly with their connection length determined by the exponential distribution. To maintain the balance of excitation and inhibition during neuronal activity, the layers of pyramidal neurons and interneurons communicate bidirectionally. Astrocytes generating calcium signals are connected by local gap junction diffusive couplings. To design the neuronal and astrocytic layers interaction, we followed the approach proposed in our previous works [37], [38]. Calcium elevations occur in response to the increased concentration of the neurotransmitter released by pyramidal neurons when a group of them fire coherently. In turn, gliotransmitters are released by activated astrocytes modulating the strength of the synaptic connections in the corresponding neuronal group. The output signal is taken from frequencies of transient discharges of pyramidal neurons.

A detailed information concerning the models and the description of parameters is provided in the Section V.

## V. Model details

In this section, the SNAN architecture is described in detail together with the STDP learning rule and neuron/astrocytic models. Specifically, we start with biological realistic models of neuronal, astrocytic networks that capture the essence of the biological interplay between these cells, at the same time minimising the computational overhead. Then we describe a communication between pyramidal neurons and astrocytes at tripartite synapses.

*1) Neural network:* Among the many existing biological plausible spiking neuron models [39]–[42], we have chosen simplified Izhikevich model [43] as computationally efficient

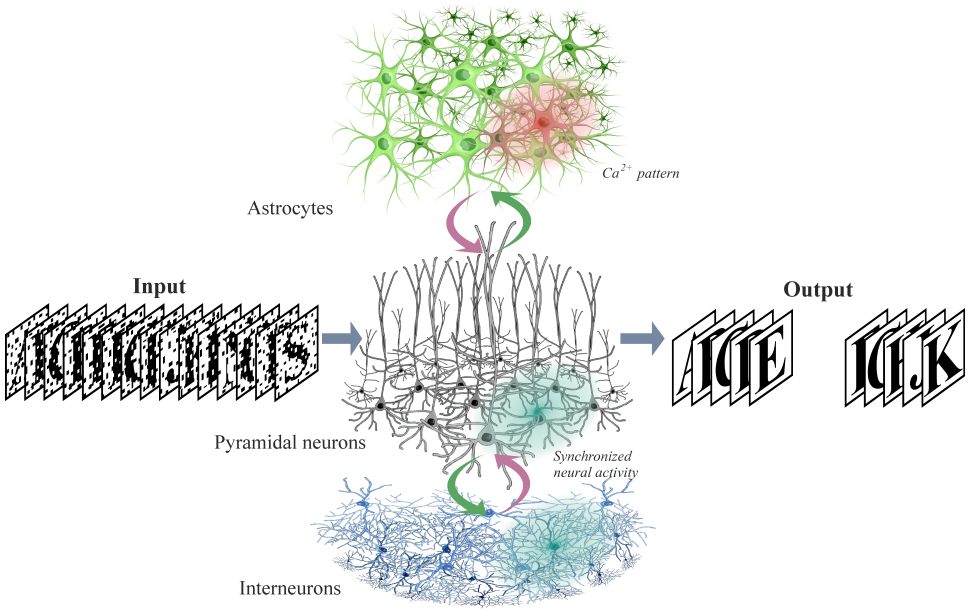


Fig. 2. Concept of situation-based memory operation in the spiking neuron-astrocyte network model.

for modeling networks. The dynamics of neuronal membrane potential is given by [43]:

$$\begin{aligned} \frac{dV_i}{dt} &= 0.04V_i^2 + 5V_i - U_i + 140 + I_{\text{app,i}} + I_{\text{syn,i}}; \\ \frac{dU_i}{dt} &= a(bV_i - U_i); \end{aligned} \tag{1}$$

with the auxiliary after-spike resetting

$$\text{if } V_i \geq 30 \text{ mV, then } \begin{cases} V_i \leftarrow c \\ U_i \leftarrow U_i + d, \end{cases} \tag{2}$$

where the subscript $i$ corresponds to the neural index, $V_i$ is the neuronal membrane potential in mV, time $t$ in ms. The applied current $I_{\text{app,i}}$ simulates the input signal, $I_{\text{syn,i}}$ is the synaptic current. The parameter descriptions and their values used in this work can be found in Table I.

The total synaptic current injected from all synapses of $i^{th}$ neuron is described by [44], [45]:

$$I_{syn,i} = \sum_{k=1}^{N_i} \frac{w_{syn,k}(E_{\text{syn}} - V_i)}{1 + \exp(-V_{\text{pre,k}}/k_{\text{syn}})}, \tag{3}$$

where $N_i$ is the total number of synapses, $w_{syn,k}$ is the weight of the $k^{th}$ synapse associated with neuron, $V_{\text{pre}}$ is the membrane potential of the presynaptic neuron, $E_{\text{syn}}$ is the synaptic reversal potential. $E_{\text{syn}} = -90$ mV for the inhibitory synapse and $E_{\text{syn}}$ = 0 mV for the excitatory. Parameter $k_{\text{syn}}$ denotes the slope of synaptic activation function threshold. We neglect the synaptic and axonal delays in system for simplicity.

Pyramidal neurons interact with each other (connection type: EE) and with interneurons (EI). Interneurons communicate with pyramidal neurons (IE) and are not interconnected. The architecture of synaptic connections between neurons is non-specific (random) with different parameters within excitatory and inhibitory layers, as well as between layers, which is described further below. A detailed list of parameters values of synaptic connection organisation can be found in Table I. The number of output connections per each neuron is fixed at $N_{out}$. Each postsynaptic neuron is randomly selected in polar coordinates. The distances between neurons $r$ are determined by the exponential distribution $f_R(r)$, and the angles $\phi$ are chosen from a uniform distribution in the range $[0; 2\pi]$:

$$f_R(r) = \begin{cases} 1/\lambda \exp(-r/\lambda), r \geq 0, \\ 0, r < 0. \end{cases} \tag{4}$$

Taking into account the difference in the sizes of the layers, the coordinates of postsynaptic neurons are calculated as follows:

$$\begin{aligned} EE: x_{post} &= \lceil x_{pre} + r\cos(\phi) \rceil, \\ y_{post} &= \lceil y_{pre} + r\sin(\phi) \rceil; \\ EI: x_{post} &= \lceil K_1^{-1} x_{pre} + r\cos(\phi) \rceil, \\ y_{post} &= \lceil K_2^{-1} y_{pre} + r\sin(\phi) \rceil; \\ IE: x_{post} &= \lceil K_1 x_{pre} + r\cos(\phi) \rceil, \\ y_{post} &= \lceil K_2 y_{pre} + r\sin(\phi) \rceil, \end{aligned} \tag{5}$$

where $x_{pre}$, $y_{pre}$ denote the coordinates of the presynaptic neuron, $x_{post}$, $y_{post}$ are the coordinates of the postsynaptic neurons, $K_1 = W/W_1$, $K_2 = H/H_1$. Coordinates are picked repeatedly in case of duplicated connection (random selection was a process without replacement).

In the proposed SNAN, the synaptic weights dynamically adjust during training only for EE and IE types of synaptic connections. The synaptic weights for EI synapses are fixed and equal to $w_{synEI}$ = 0.1. The initial weights of the synapses between pyramidal neurons (EE) and interneuron–pyramidal neuron (IE), are $10^{-4}$. The maximum weights are limited to values $w_{synEEmax}, w_{synIEmax}$. The STDP rule updates the

synaptic weights according to the timing difference between the pre and postsynaptic spikes, and is described by:

$$\delta w_{synEE,k}(\Delta t) = \begin{cases} g_{synEE}\exp(\Delta t/\tau),\ \Delta t \le 0, \\ -g_{synEE}\exp(\Delta t/\tau),\ \Delta t > 0; \end{cases} \quad (6)$$
$$w_{synEE,k} \in [10^{-4}, w_{synEEmax}],$$

where $\delta w_{synEE,k}(\Delta t)$ is used to update the synaptic weight, $\Delta t$ is the time difference between presynaptic and postsynaptic spikes, $g_{synEE}$ is the plasticity window height, $\tau$ control the width of the plasticity window, and they are 20 ms in our model. Training of synaptic connections from interneurons to pyramidal neurons is organized so that interneurons activated by pyramidal neurons inhibit all subnetwork of pyramidal neurons that were not active during the presentation of the training pattern. In such way, the weights of IE synapses are updated according the following:

$$\delta w_{synIE,k}(\Delta t) = \begin{cases} g_{synIE}\exp(\Delta t/\tau)H(f^* - f),\ \Delta t \le 0, \\ -g_{synIE}\exp(\Delta t/\tau),\ \Delta t > 0; \end{cases}$$
$$w_{synIE,k} \in [10^{-4}, w_{synIEmax}], \quad (7)$$

where $\Delta t$ is the time difference between presynaptic and postsynaptic spikes, $g_{synIE}$ is the plasticity window height, $\tau$ control the width of the plasticity window, and they are 20 ms in our model. $f$ and $f^*$ are the actual firing rate (i.e. a running average over 10 ms) and threshold firing rate of the postsynaptic pyramidal neuron, respectively. $H$ is the Heaviside step function.

*2) Astrocytic network:* The astrocytic layer consists of 676 cortical astrocytes connected with only nearest neighbors. It has been experimentally shown that an individual cortical astrocyte contacts on several neuronal somatas and hundreds neuronal dendrites with some overlapping in the spatial territories corresponding to different astrocytes in the cortex [46]. Such an organization of neuron-astrocyte interaction allows the astrocytes to integrate and coordinate a unique volume of synaptic activity. Following experimental evidences, each astrocyte in the SNAN bidirectionally interacts with ensemble of $N_{AE}$=16 pyramidal neurons with some overlapping. Spiking neuronal activity induces the release of neurotransmitter (glutamate) from the presynaptic terminals into the synaptic gap. The released glutamate binds to the metabotropic glutamate receptors (mGluRs) on the astrocyte membrane and triggers the production of inositol 1,4,5-trisphosphate ($IP_3$) in astrocytes, which is followed by the generation of a calcium pulse. The Ullah model [47] is used to describe the dynamics of the intracellular concentrations of $IP_3$ and $Ca^{2+}$ in astrocytes:

$$\begin{aligned} \frac{d[Ca^{2+}]_m}{dt} &= J_{\text{ER}} - J_{\text{pump}} + J_{\text{leak}} + J_{\text{in}} - J_{\text{out}} + J_{\text{Gca}}; \\ \frac{dh_m}{dt} &= a_2\left(d_2\frac{[IP_3]_m + d_1}{[IP_3]_m + d_3}(1 - h_m) - [Ca^{2+}]_m h_m\right); \\ \frac{d[IP_3]_m}{dt} &= \frac{[IP_3]^* - [IP_3]_m}{\tau_{IP3}} + J_{\text{PLC}\delta} + J_{\text{glu}} + J_{\text{Gip3}} \end{aligned} \quad (8)$$

where $m$ ($m$ = 1, …, 676) is the astrocyte index. $[Ca^{2+}], [IP_3], h$ are the cytosolic calcium and $IP_3$ concentrations and fraction of activated $IP_3$ receptor on the endoplasmic reticulum (ER) membrane, respectively. $J_{ER}$ is $Ca^{2+}$ flux from the ER to the cytosol, $J_{pump}$ is the pump flux from cytosol to ER, $J_{leak}$ is the leakage flux from the ER to the cytosol. The fluxes $J_{in}$ and $J_{out}$ describe the exchange of calcium with the extracellular space. $J_{\text{PLC}\delta}$ describes the production of $IP_3$ by phospholipase C$\delta$ (PLC$\delta$), $J_{glu}$ describes the glutamate-induced $IP_3$ production in response to neural activity. These fluxes are expressed as follows:

$$\begin{aligned} J_{\text{ER}} &= c_1 v_1 [Ca^{2+}]^3 h^3 [IP_3]^3 \frac{\left(c_0/c_1 - (1 + 1/c_1)[Ca^{2+}]\right)}{\left(([IP_3] + d_1)([Ca^{2+}] + d_5)\right)^3}; \\ J_{\text{pump}} &= \frac{v_3 [Ca^{2+}]^2}{k_3^2 + [Ca^{2+}]^2}; \\ J_{\text{leak}} &= c_1 v_2 \left(c_0/c_1 - (1 + 1/c_1)[Ca^{2+}]\right); \\ J_{\text{in}} &= \frac{v_6 [IP_3]^2}{k_2^2 + [IP_3]^2}; \\ J_{\text{out}} &= k_1 [Ca^{2+}]; \\ J_{\text{PLC}\delta} &= \frac{v_4\left([Ca^{2+}] + (1 - \alpha)k_4\right)}{[Ca^{2+}] + k_4}. \end{aligned} \quad (9)$$

Astrocytes interact with each other through gap junctions. Gap junctions are permeable to the second messenger $IP_3$ and to calcium ions [48], [49]. Currents $J_{\text{Gcam}}$ and $J_{\text{Gip3m}}$ describe the diffusion of $Ca^{2+}$ ions and $IP_3$ molecules via gap junctions of the $m$th astrocyte and can be expressed as follows:

$$\begin{aligned} J_{\text{Gcam}} &= d_{ca}\sum_j([Ca^{2+}]_j - [Ca^{2+}]_m); \\ J_{\text{Gip3m}} &= d_{ip3}\sum_j([IP_3]_j - [IP_3]_m); \end{aligned} \quad (10)$$

where $j$, $d_{ca}$ and $d_{ip3}$ represent, respectively, the number of astrocytes connected to the $m$th astrocyte and the $Ca^{2+}$ and $IP_3$ diffusion rates. Biophysical meaning of all parameters in Eqs. (8), (9), (10) and their values can be found in [47] and are summarised in Table II (astrocytic network parameters). Note that the timescale of the model of calcium dynamics in astrocyte is seconds. At the same time, the timescale of model (1), (2) is milliseconds. To match the timescales in the combined model we had to appropriately rescale the values of relevant model parameters.

*3) Bidirectional neuron-astrocyte interaction:* The amount of neurotransmitter-glutamate that diffuses from the synaptic cleft associated with the $i$th pyramidal neuron and reaches the astrocyte is described by the following equation [26], [50]:

$$\frac{dG_i}{dt} = -\alpha_{\text{glu}} G_i + k_{\text{glu}} H\left(V_i - 30mV\right), \quad (11)$$

where $\alpha_{\text{glu}}$ is the glutamate clearance constant, $k_{\text{glu}}$ is the release efficiency, $H$ is the Heaviside step function, and $V_i$ is the membrane potential of $i$th pyramidal neuron. Glutamate contacts the mGluRs on the astrocyte membrane and initiates the production of $IP_3$. The flux $J_{glu}$ represents the glutamate-induced $IP_3$ production and is defined as follows:

$$J_{\text{glu}} = \begin{cases} A_{\text{glu}}, & \text{if} \quad t_0 < t \le t_0 + t_{\text{glu}}, \\ 0, & \text{otherwise}; \end{cases} \quad (12)$$

here $t_0$ represents the moment when the total level of glutamate concentration in all synapses associated with this astrocyte reaches a threshold:

$$\left(\frac{1}{N_{AE}}\sum_{i\in N_{AE}}\left[G_i \geq G_{\text{thr}}\right]\right) \geq F_{act}, \tag{13}$$

where the parameter $G_{\text{thr}} = 0.2$ is the threshold for glutamate, $[x]$ is the Iverson bracket. $F_{\text{act}} = 0.75$ denotes the fraction of synchronously spiking neurons of the neuronal ensemble corresponding to the astrocyte.

Experimental studies have shown that astrocytes are able to facilitate synaptic transmission due to the action of glutamate released from astrocytes. More precisely, we consider that the astrocytic glutamate induces potentiation of the excitatory synapse via NMDAR-dependent postsynaptic slow inward currents (SICs) generation [51], [52] and mGluR-dependent heterosynaptic facilitation of presynaptic glutamate release [53]–[55]. In the SNAN, we propose that $Ca^{2+}$ elevation in astrocytes results in glutamate release, which can modulate the synaptic strength of all synapses corresponding to the morphological territory of a given astrocyte. For simplicity, astrocyte-induced enhancement of synaptic weight of the affected excitatory synapses, $\overline{w_{synEE}}$, is described as follows:

$$\begin{aligned}\overline{w_{synEE}} &= w_{synEE}\ \left(1+\nu_{Ca}\right), w_{synEE}\in[0, w_{synEEmax}]\\ \nu_{Ca} &= \nu^*_{Ca} H\left([Ca^{2+}]_m - [Ca^{2+}]_{\text{thr}}\right),\end{aligned} \tag{14}$$

where $w_{synEE}$ is the weight of the excitatory synapse trained according to Hebb's rule, $\nu^*_{Ca}$ = 2 represents the strength of the astrocytic modulation of the synaptic weight, $H(x)$ is the Heaviside function, $[Ca^{2+}]_{\text{thr}}$ denotes the threshold $Ca^{2+}$ concentration in the astrocyte $m$. The feedback from the astrocytes to the neurons is activated when the astrocytic $Ca^{2+}$ concentration is larger than $[Ca^{2+}]_{\text{thr}}$, and the fraction of synchronously spiking neurons of neuronal ensemble corresponding to the astrocyte $F_{\text{astro}}$ during the period of $\tau_{\text{syn}}$ = 5 ms. The duration of astrocyte-induced enhancement of synaptic transmission is fixed and equal to $\tau_{\text{astro}}$ = 20 ms.

Model equations are integrated using the Runge-Kutta fourth-order method with a fixed time step, $\Delta t = 0.1$ ms. A detailed listing of model parameters and values can be found in Tables I (neural network model), II (astrocytic network parameters), III (neuron-astrocytic interaction parameters) and IV (training and testing protocol parameters). The code is available at https://github.com/altergot/Neuron-astrocyte-network-Situation-associated-memory.

## VI. Memory performance metrics

To measure the memory performance of the proposed SNAN, we used the following correlation-like quantity $C(t)$ computing the similarity between recalled (actual) and intended (ideal) patterns:

$$\begin{aligned}M_i(t) &= I\left[\left(\sum_{k\in[t-w,t]} I\left[V_i(k)\geq 30\ mV\right]\right) > 0\right],\\ C(t) &= \frac{1}{2}\left(\frac{1}{N_s}\sum_{i\in S} M_i(t) + \frac{1}{N_{ns}}\sum_{i\notin S}\left(1-M_i(t)\right)\right).\end{aligned} \tag{15}$$

In (15), $M_i(t)$ is equal to 1 if the $i$-th pyramidal neuron produces a spike within the interval $[t-w, t]$ (with $w$ = 1ms), otherwise $M_i(t)$ is set to 0; $S$ is the set of non-zero pixels representing or encoding the ideal sample ($N_s$ is their number), $N_{ns} = (W \cdot H - N_s)$ is the number of pixels that do not belong to the ideal sample; $W$, $H$ are the dimensions of the pyramidal neuron layer (width and height, respectively); $I$ in (15) is the indicator function. The correlation metric $C(t)$ can be related to the Hamming distance $d$ between the ideal and the recalled patterns.

For each $j$-th pattern, we computed their corresponding correlation values $C_j(t)$. This was then followed by determining their maximal values over the finite interval (tracking range) $[t-T_P, t]$, $T_P$=30ms, and averaging over the set of all test patterns:

$$C_{test}(t) = \frac{1}{N_{test}}\sum_{j=1}^{N_{test}} \max_{\tau\in[t-T_P,t]} C_j(\tau), \tag{16}$$

where $N_{test}$ is the number of test patterns.

### A. Training and Testing Protocol

To train and test the proposed SNAN, we use the alpha-digits data set (https://github.com/altergot/Neuron-astrocyte-network-Situation-associated-memory/tree/main/images) which consists of $P$ binary images of digits and capital letters of size $W \times H$ pixels. The input patterns are fed to the layer of pyramidal neurons. Each image pixel corresponds to a neuron, which receives a rectangular excitatory pulse, $I_{app,i}$, with length $t_{stim}$ and amplitude $A_{stim}$ for training (with $t_{test}$ and $A_{test}$ in case of testing). On average there are 950 neurons under stimulation (15% of the network) in a training image. Training samples were presented to highly overlapped neuronal populations (an average for 40 training samples overlapping was 51%). The output signal was read out according to the firing rates of pyramidal neurons.

*1) SNN pre-training:* First, we pre-trained the synaptic connections only in the spiking neuronal network consisting of pyramidal neurons and interneurons without taking into account the influence of astrocytes. During pre-training, each of $P$ patterns was presented to the neuronal network 10 times in random order. After the pre-training was completed, the network weights were fixed. To test the training quality, we calculated the correlation of recalled patterns with the ideal samples according to the procedure described in VI. In the cued recall, we applied a shorter inputs with lower amplitude ($t_{test}$, $A_{test}$) to the network. These inputs were spatially distorted by high-level random noise matching the training samples.

*2) Situation-based learning in SNAN:* To implement the situation-based learning in the proposed SNAN, we use the following protocol. After the SNN pre-training, we turn on the bidirectional interaction between pyramidal neuron layer and astrocytic layer. To let the astrocytic network generate the first calcium pattern, we apply the initial pool of patterns to SNAN. This pool consists of 7 (seven) randomly selected patterns from the general data set used in the SNN pre-training. Each pattern was presented 10 (ten) times.

TABLE I
NEURAL NETWORK PARAMETERS ( [43], [44])

| Parameter | Parameter description | Value |
|---|---|---|
| $W \times H$ | pyramidal neurons layer grid size | $79 \times 79$ |
| $W_1 \times H_1$ | interneurons layer grid size | $40 \times 40$ |
| $a$ | time scale of the recovery variable | 0.1 |
| $b$ | sensitivity of the recovery variable to the sub-threshold fluctuations of the membrane potential | 0.2 |
| $c$ | after-spike reset value of the membrane potential | -65 mV |
| $d$ | after-spike reset value of the recovery variable | 2 |
| $\eta$ | synaptic weight without astrocytic influence | 0.025 |
| $E_{\text{syn}}$ | synaptic reversal potential for excitatory synapses | 0 mV |
| | synaptic reversal potential for inhibitory synapses | -90 mV |
| $k_{\text{syn}}$ | slope of the synaptic activation function | 0.2 mV |
| | **Connections within a pyramidal neurons layer:** | |
| $N_{\text{outEE}}$ | number of output connections per each neuron | 200 |
| $\lambda_{\text{EE}}$ | rate of the exponential distribution of synaptic connections distance | 15 |
| $g_{synEE}$ | change in the value of the weight during training | 0.007 |
| $w_{synEEmax}$ | maximum synaptic weight | 0.05 |
| | **Connections from a pyramidal neurons layer to interneurons layer:** | |
| $N_{\text{outEI}}$ | number of output connections per each neuron | 5 |
| $\lambda_{\text{EI}}$ | rate of the exponential distribution of synaptic connections distance | 2 |
| $w_{synEI}$ | weight of synaptic connections | 0.1 |
| | **Connections from a interneurons layer to pyramidal neurons layer:** | |
| $N_{\text{outIE}}$ | number of output connections per each neuron | 2000 |
| $\lambda_{\text{IE}}$ | rate of the exponential distribution of synaptic connections distance | 80 |
| $g_{synIE}$ | change in the value of the weight during training | 0.007 |
| $w_{synIEmax}$ | maximum synaptic weight | 0.05 |
| $f^*$ | the threshold firing rate of the pyramidal neuron for training of IE connections | 0.3 |

Noise is an essential part of both sensory input [57] and internal neuronal dynamics and may contribute to information processing in neural systems as well as to learning and memory [58]. Noise can play a role of a regularizer in training deep learning neural networks too [59]. Recent work demonstrated that external noise in SNN-based learning systems could help to maintain and recover memorized patterns [60]. Given the ubiquity and relevance of noise, we corrupted the input training patterns by a random 5% "salt and pepper" noise. After a break (approximately 650 ms) needed for the formation of calcium impulses in pattern-associated astrocytes, we started the ongoing training-testing process of the SNAN in real time. This situation-based learning process can be conventionally divided into a sequence of cycles, which follow each other continuously.

Every test cycle starts with training of the SNAN on one new pattern which was absent in the initial pool and was randomly chosen from the general data set. After that, we test the storage of all patterns from the initial pool in memory.

TABLE II
ASTROCYTIC NETWORK PARAMETERS [47]

| Parameter | Parameter description | Value |
|---|---|---|
| $M \times N$ | astrocytic network grid size | $26 \times 26$ |
| $c_0$ | total $Ca^{2+}$ in terms of cytosolic vol | 2.0 $\mu$M |
| $c_1$ | (ER vol)/(cytosolic vol) | 0.185 |
| $v_1$ | max $Ca^{2+}$ channel flux | 6 $s^{-1}$ |
| $v_2$ | $Ca^{2+}$ leak flux constant | 0.11 $s^{-1}$ |
| $v_3$ | max $Ca^{2+}$ uptake | 2.2 $\mu$M $s^{-1}$ |
| $v_6$ | maximum rate of activation dependent calcium influx | 0.2 $\mu$M $s^{-1}$ |
| $k_1$ | rate constant of calcium extrusion | 0.5 $s^{-1}$ |
| $k_2$ | half-saturation constant for agonist-dependent calcium entry | 1 $\mu$M |
| $k_3$ | activation constant for ATP-$Ca^{2+}$ pump | 0.1 $\mu$M |
| $d_1$ | dissociation constant for $IP_3$ | 0.13 $\mu$M |
| $d_2$ | dissociation constant for $Ca^{2+}$ inhibition | 1.049 $\mu$M |
| $d_3$ | receptor dissociation constant for $IP_3$ | 943.4 nM |
| $d_5$ | $Ca^{2+}$ activation constant | 82 nM |
| $\alpha$ | | 0.8 |
| $v_4$ | max rate of $IP_3$ production | 0.3 $\mu$M $s^{-1}$ |
| $1/\tau_r$ | rate constant for loss of $IP_3$ | 0.14 $s^{-1}$ |
| $[IP_3]^*$ | steady state concentration of $IP_3$ | 0.16 $\mu$M |
| $k_4$ | dissociation constant for $Ca^{2+}$ stimulation of $IP_3$ production | 1.1 $\mu$M |
| $d_{ca}$ | $Ca^{2+}$ diffusion rate | 0.05 $s^{-1}$ |
| $d_{ip3}$ | $IP_3$ diffusion rate | 0.05 $s^{-1}$ |

TABLE III
NEURON-ASTROCYTIC INTERACTION PARAMETERS [50]

| Parameter | Parameter description | Value |
|---|---|---|
| $N_{AE}$ | number of neurons interacting with one astrocyte | 16, $4 \times 4$ |
| $\alpha_{\text{glu}}$ | glutamate clearance constant | 50 $s^{-1}$ |
| $k_{\text{glu}}$ | efficacy of the glutamate release | 600 $\mu$M $s^{-1}$ |
| $A_{glu}$ | rate of $IP_3$ production through glutamate | 5 $\mu$M $s^{-1}$ |
| $t_{\text{glu}}$ | duration of $IP_3$ production through glutamate | 60 ms |
| $G_{\text{thr}}$ | threshold concentration of glutamate for $IP_3$ production | 0.2 |
| $F_{\text{act}}$ | fraction of synchronously spiking neurons required for the emergence of $Ca^{2+}$ elevation | 0.75 |
| $F_{\text{astro}}$ | fraction of synchronously spiking neurons required for the emergence of astrocytic modulation of synaptic transmission | 0.5 |
| $\nu^*_{Ca}$ | strength of the astrocyte-induced modulation of synaptic weight | 2 |
| $[Ca^{2+}]_{\text{thr}}$ | threshold concentration of $Ca^{2+}$ for the astrocytic modulation of synapse | 0.15 $\mu$M |
| $\tau_{\text{astro}}$ | duration of the astrocyte-induced modulation of synapse | 20 ms |

TABLE IV
TRAINING AND TESTING PROTOCOL PARAMETERS

| Parameter | Parameter description | Value |
|---|---|---|
| $A_{\text{stim}}$ | stimulation amplitude in training | 80 $\mu$A |
| $t_{\text{stim}}$ | stimulation duration in training | 2 ms |
| $t_{\text{between stim}}$ | time between patterns in training | 3 ms |
| | noise level in training | 5% |
| $A_{\text{test}}$ | stimulation amplitude in test | 8 $\mu$A |
| $t_{\text{test}}$ | stimulation length in test | 20 ms |
| $t_{\text{between test}}$ | time between patterns in test | 50 ms |
| | noise level in test | 20% |
| $P$ | number of pre-training patterns | 40; 20 |

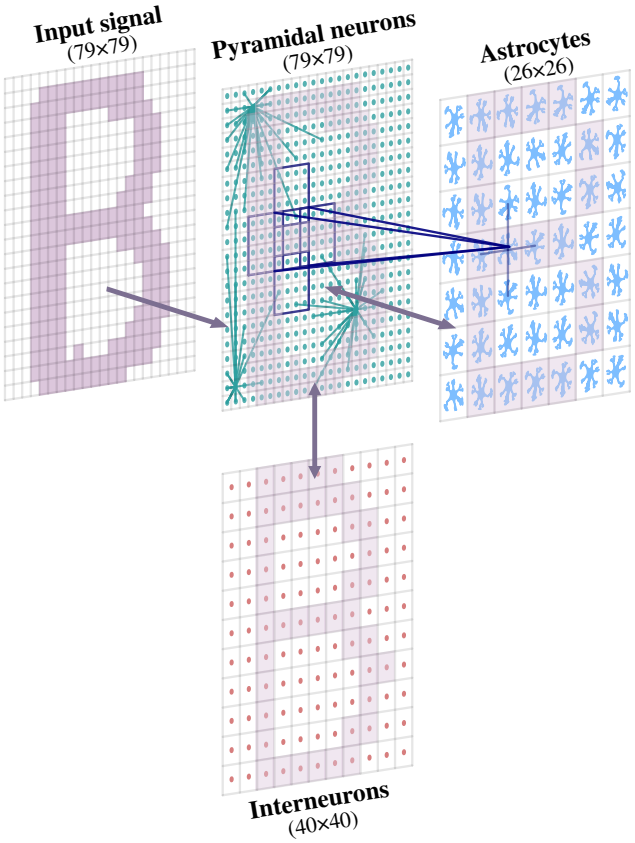


Fig. 3. A spiking neuron-astrocyte network topology. The SNAN includes three interacting layers: the layer of pyramidal neurons, the layer of interneurons, and the astrocytic layer. First layer ($79 \times 79$) consists of synaptically coupled pyramidal neurons. The pyramidal neurons bidirectionally communicate with the interneurons from the second layer ($40 \times 40$). Ratio of pyramidal neurons to interneurons in the model is chosen in accordance with the experimental observations and computational model of the cortex [56], where 80% of the CSN neurons are pyramidal neurons and 20% are interneurons. Astrocytes are connected by a local gap junction diffusive couplings and represent a two-dimensional square lattice with a dimension $26 \times 26$. We focus on the bidirectional interaction between the first neuronal and astrocytic layers. Each astrocyte is interconnected with an ensemble of $N_a = 16$ pyramidal neurons with dimensions $4 \times 4$ (red lines) with overlapping in one row and one column. An input signal encoded as a two-dimensional pattern is applied to the first layer.

Throughout the article, we use the term 'memory' referring to the ability of pattern recall in presence of perturbations. We present the SNAN with the 7 test patterns which match the patterns from the initial pool, but have a shorter lengths, lower amplitude ($t_{test}$, $A_{test}$) and which are spatially distorted by high level (20%) random noise. To identify the memory performance, we analyze the quality of the recalled patterns. In the next cycle, one pattern from the initial pool is replaced by a new pattern which has been learned in the previous cycle. Thus, after 7 cycles all patterns from the initial pool are substituted by new patterns from the general pre-training data set. This procedure can be performed endlessly allowing the system to work with all patterns from the general data set in a situation-based mode. Figure 4 illustrates the time scheme of the training and testing protocol. The values of the stimulation parameters are listed in Table IV.

## VII. Results

### A. SNN memory performance

First, we determine the size of the general data set that can be loaded in memory of the SNN and used for implementation of the situation-based learning in the proposed SNAN. For this, we pre-train the SNN on the data set of different sizes and test the quality of memory maintenance of the SNN in cued recall. Information retrieval is organized by the application of a cue sample representing one pattern from the memory set distorted by "salt and pepper" noise. The dependencies of the correlation between the SNN cued recalls and the ideal target samples (averaged over all test patterns $\pm$ standard deviation) on the data set size are shown in Fig. 5 by red curves. Two cases were considered for test images distorted by 20% (Fig. 5a) and 30% (Fig. 5b) noise levels. The maximum correlations between SNN recalls and non-target sample averaged over all test patterns and the maximum correlation between target and non-target samples are presented by blue and green curves in Fig. 5, respectively. According to the results obtained, the considered SNN can learn up to 40 patterns. In further analysis, we used data set sizes of 20 and 40 patterns for comparison.

### B. SNAN situation-based learning performance

*1) Astrocytic contribution to the SNAN memory performance:* To assess the contribution of astrocytes in information processing and memory formation in neuron-astrocyte networks, the pre-trained SNN was bidirectionally connected to the astrocytic layer. To start the process of the SNAN situation-based learning, we load the initial pool of 7 patterns to the system by applying the inputs (Fig. 6A, D, G) to the pyramidal neuronal layer. The activity of pattern-specific neuronal subnetworks (Fig. 6B, E, H) induces the generation of calcium signals in corresponding astrocytes. Due to the fact that calcium dynamics in astrocytes has slow scale, the overlapped spatial calcium patterns in astrocytic layer for different samples coexist for several seconds (Fig. 6C, F, I).

Then we ran the ongoing process of situation-based learning according to the approach described in the Section VI-A2 and illustrated in Fig. 4. Briefly, in each of the 10 cycles, we loaded a new pattern from pre-training data set to the SNAN and tested the patterns memorized in the previous cycles. A constant number of patterns in the cycle was maintained by deleting one randomly selected pattern during each cycle. Test patterns were applied to the pyramidal neurons with 20 % level noise, and the SNANs cued recalls in the values of the neuronal firing rate were read out. Examples of input test images from several cycles and the systems retrievals are shown in Fig. 7.

To estimate the astrocytic impact on the memory formation in the SNAN, we calculated the dependencies of recall correlation with samples on the noise level. First the test was run with astrocytic modulation of synaptic transmission in the SNN and then without it (Fig. 8). The test involved 20 and 40 patterns from the pre-trained data set. The differences in correlation between the recalled pattern and noisy input clearly show that astrocytes steadily improve the quality of the system retrieval

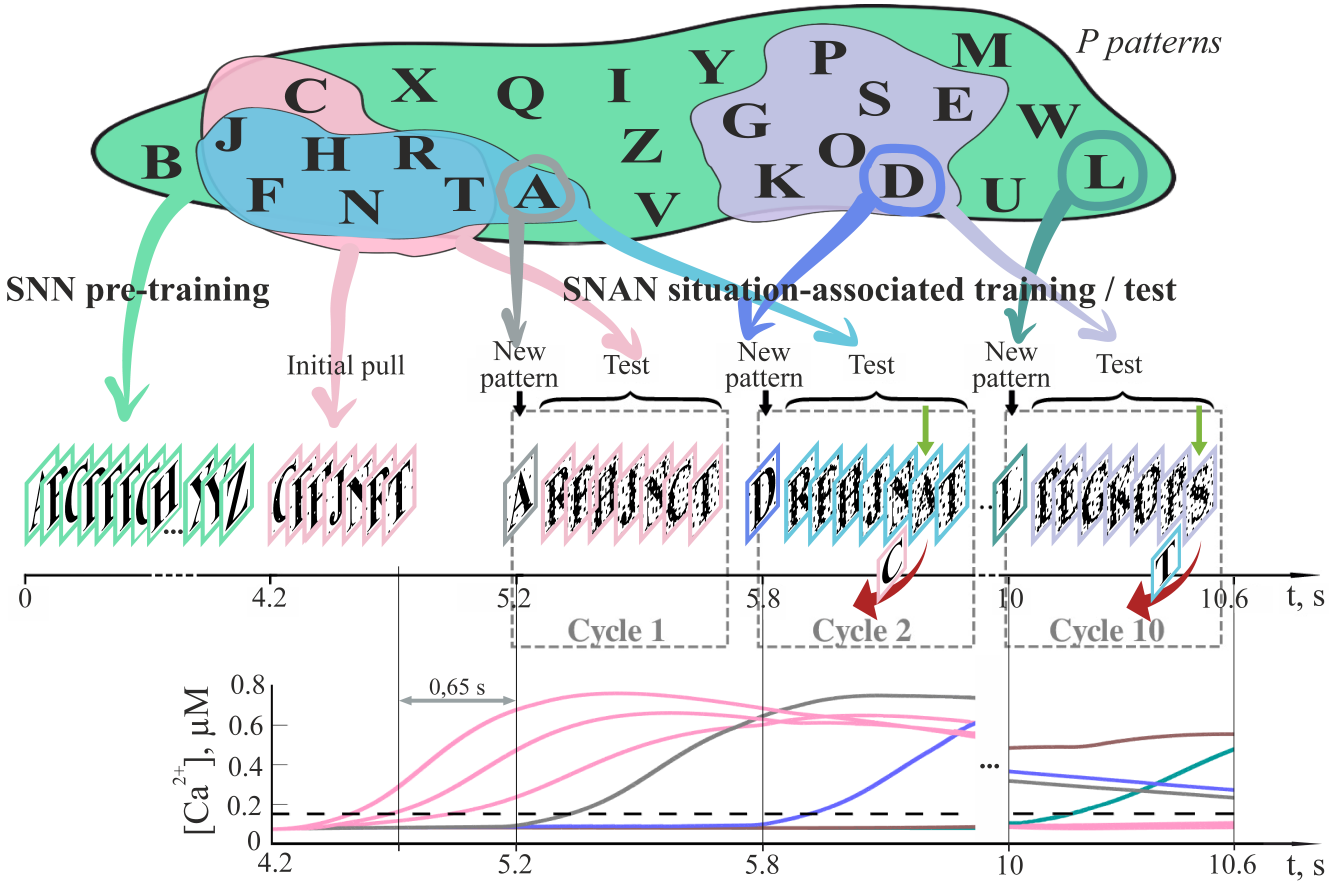


Fig. 4. Training and testing protocol. For training and testing of the proposed SNAN we use the alpha-digits data set consisting of $P$ binary images of digits and capital letters. The input patterns are fed to the layer of pyramidal neurons. First, we pre-train the spiking neuronal network consisting of pyramidal neurons and interneurons without taking into account the influence of astrocytes. During pre-training, each $P$ pattern is presented to the neuronal network 10 times in random order (green color). After the pre-training is completed, the synaptic weights are fixed. To implement the situation-based learning in the proposed SNAN, we use the following protocol. After the SNN pre-training, we turn on the bidirectional interaction between pyramidal neurons and astrocytic layers. To let the astrocytic network generate the first calcium pattern, we apply the initial pool of patterns to SNAN. This pool consists of 7 (seven) randomly selected patterns (pink color) from the general data set used in the SNN pre-training. Each pattern is presented 10 times with the addition of a random 5% "salt and pepper" noise. After a break (approximately 650 ms) necessary for the formation of calcium elevations in the pattern-specific astrocytes (examples of astrocytic $Ca^{2+}$ signals are shown in colors corresponding to the patterns), we start ongoing training-testing process of the SNAN in real time. This situation-based learning process can be conventionally divided into a sequence of cycles, which follow each other continuously. Every test cycle starts with training of the SNAN on one new pattern (e.g. pattern "A", grey color), which was absent in the initial pool and was randomly chosen from the general data set. After that, we test the memorization of all patterns from the initial pool - "Cycle 1". We present the SNAN with test patterns which have been spatially distorted by high-level noise. To identify the memory performance, we analyze the quality of the recalled patterns. In the next cycle, "Cycle 2", one pattern from the initial pool (pattern "C") is replaced by new pattern which has been learned in the previous cycle (pattern "A"), this models situation-based environment. Thus, after $N$ cycles all patterns from the initial pool are substituted by new patterns from the general pre-training data set. This procedure can be performed endlessly allowing the system to work with all patterns from the general data set in situation-based mode.

up to 10% for high noise levels (red curve in comparison with blue curve). The reason for such recalls enhancement is that a short presentation of the cue to the neural network evokes the additional astrocytic-induced spike in the synaptic strength between stimulus-specific neurons, which results in a local spatial synchronization in the whole stimulus-specific neuronal population.

*2) Contribution of the SNN pre-training to the SNAN memory performance:* Next, we evaluate the contribution of the neural network learning to the SNAN memory performance according to synaptic weights adjustment via the STDP rule. For this, we compare the memory performance of the three SNAN types (i) with synaptic connections trained according to the STDP rule, (ii) with randomly mixed synaptic weights after the SNN pre-training, and (iii) with fixed synaptic weights without the SNN pre-training. Figure 9(A) shows the changes in the correlation of the SNANs cued retrievals relative to the input noise patterns for these cases with and without astrocytic influence on neural activity. The best levels of recall correlations were demonstrated by the proposed SNAN trained by the STDP rule with astrocytic modulation of synaptic transmission, followed by the SNAN with mixed synaptic weights and astrocytic modulation, and then the pre-trained SNN without astrocytes. The worst results were shown by networks without astrocytic modulation of synaptic transmission and without training of synaptic connections. Interestingly, astrocyte-induced enhancement of synaptic transmission in the sample-specific neuronal subnetworks can provide good quality retrieval in the system even for neural networks with mixed weights of synaptic connections (blue line in Fig. 9(A)).

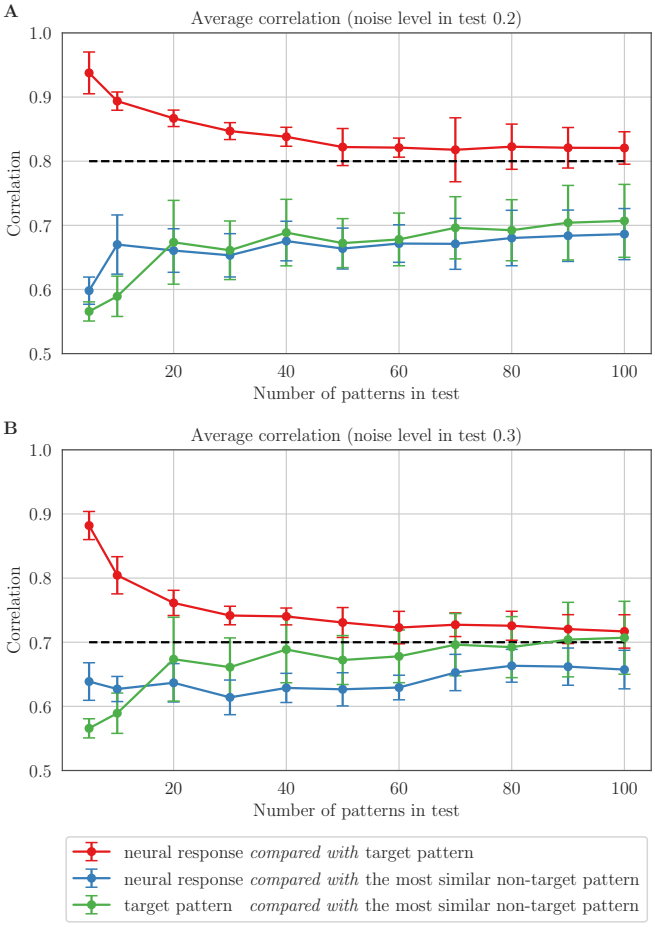


Fig. 5. The pre-trained SNN's memory performance. The correlations between SNN recalls and the ideal target samples for different data set size are marked by red. The maximum correlations between SNN recalls and non-target sample are marked by blue. The maximum correlation between target and non-target samples are marked by green. Average means over all test patterns ± standard deviation are shown for 20% (A) and 30% (B) noise levels in test images. The dotted line indicates test patterns correlation.

*3) Effect of the synaptic connectivity strength on the SNAN memory performance:* Next, we studied the influence of synaptic connectivity architecture in the neural layers of the SNAN on the correlation of the system recalls. We specifically focused on the weight of synaptic connections between layers and inside the pyramidal neuronal layer. Higher inhibition of the system (Fig. 9(B)) due to the increase of the maximum synaptic weights of the connection from interneurons layer to pyramidal neurons, $w_{synIEmax}$, induces the SNN memory performance decline (red dashed line), but does not affect the SNAN memory performance (red line). This can be explained by the fact that samples in training were applied to higly overlapped neuronal population. Such subnetworks of interneurons corresponding to several patterns provide strong inhibition of the signal propagation in sample-specific population of pyramidal neurons and prevent correct recall. However, this can be compensated by the stimul-specific astrocyte-induced enhancement of excitatory synaptic transmission. On the contrary, increasing the maximum excitatory synaptic strengths in the pyramidal neuronal layer, $w_{synEEmax}$, results in astrocyte-induced overactivation of the SNAN and a decrease in the recall quality (Fig. 9(C) red and green lines).

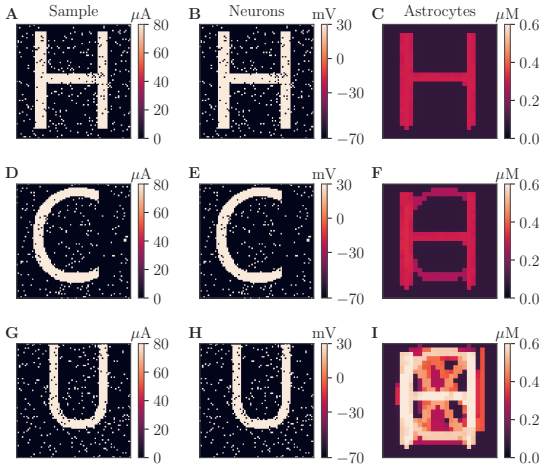


Fig. 6. The example of SNAN training on the patterns from initial pool (Figure 4). (A, D, G) The first, second, and the 7th training patterns from initial pool, respectively. (B, E, H) Responses of the pyramidal neuronal layer to the patterns. The values of the membrane potentials are shown. (C, F, I) Intracellular $Ca^{2+}$ concentrations in the astrocytic layer.

*4) Capacity of the situation-based memory in the SNAN:* The situation-based memory capacity in the proposed SNAN is determined by the duration of $Ca^{2+}$ signals in astrocytes. Duration of astrocytic $Ca^{2+}$ elevations is determined by the intrinsic mechanisms of the $IP_3$-evoked calcium release from the endoplasmic reticulum in astrocytes, which is described by the biophysical model [47] used in this study. Brief application of the cue samples during testing results in prolongation of $Ca^{2+}$ elevations in astrocytes and, thus, in the increased storage time of patterns in the memory of the SNAN. On average, the $Ca^{2+}$ signals duration in astrocytes is 3.8 s, which can support the situation-based learning during 9 cycles on 15 different patterns.

*5) Impact of the overlapping level in samples on the SNAN memory performance:* The pre-trained spiking neural network can retrieve the correct samples from test images distorted with 20% noise level with the average correlation level of 96%. This, however, applies only to non-overlapping patterns without additional effect of astrocytic modulation, since even a small sample overlapping results in chimeras generation in the solely neuronal network model. To characterize the impact of the overlapping level in training samples on the SNAN memory performance, we use rectangles of different sizes displaced at the fixed number of pixels relative to the neighbor as information patterns (Fig. 10A). In this case, in contrast to the used alpha-digit data set, the level of overlapping between the neighboring patterns can be precisely specified.

After the SNN pre-training on 40 patterns with fixed overlapping, we use the situation-based training and testing protocol for the SNAN described above with little modifications. To be sure that sample overlapping level inside one cycle is


Fig. 7. The example of the SNAN test patterns from the general pre-trained data set (Figure 4). Three testing cycles are shown. Left panel presents the testing images with 20% "salt-and-pepper" noise. Right panel presents the cued recalls in the pyramidal neuronal layer. The averaged firing rate on the test time interval for each neuron is shown.

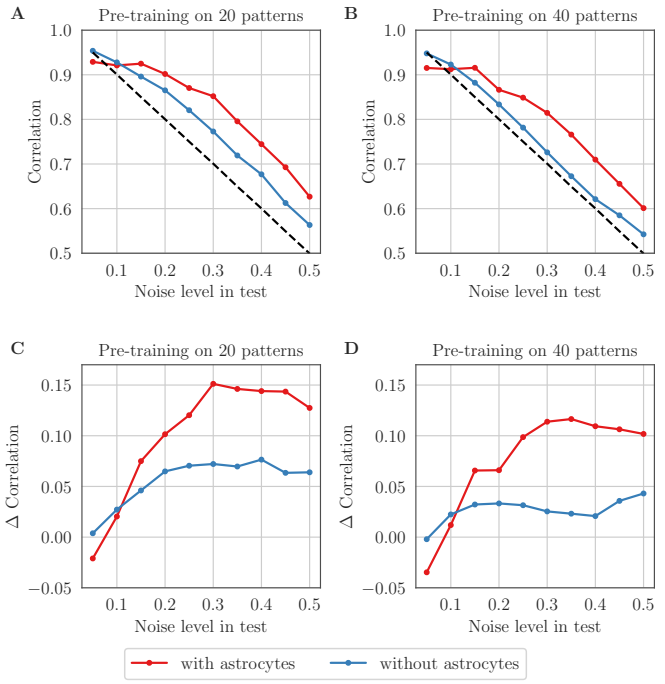


Fig. 8. The astrocyte-induced enhancement of the memory performance in the proposed SNAN. (A, B) The correlations between SNAN recalls and the ideal samples dependent on noise level in testing patterns with astrocytic modulation of synaptic transmission in neural network (red curves) and without it (blue curves). (C, D) The difference between correlations of systems recalls and test patterns. (A,C) and (B, D) correspond to data set sizes of 20 and 40 patterns, respectively. The dotted line indicates test patterns correlation.

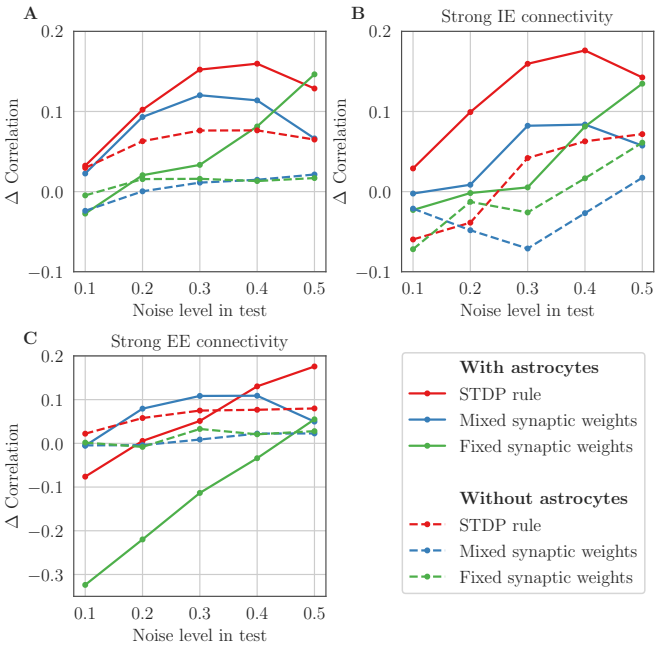


Fig. 9. The difference between correlations of the SNANs recalls and test patterns. The memory performance was shown for three SNAN types with and without astrocytic influence: (i) with synaptic connections trained according to the STDP rule, (ii) with randomly mixed synaptic weights after the SNN pre-training, and (iii) with fixed synaptic weights without the SNN pre-training. (A) $w_{synIEmax}$=0.05, $w_{synEEmax}$=0.05; (B) Strong connections from interneurons to pyramidal neurons $w_{synIEmax}$=0.15, $w_{synEEmax}$=0.05; (C) Strong connections inside the pyramidal neurons layer $w_{synIEmax}$=0.05, $w_{synEEmax}$=0.07.

constant between all patterns, we apply samples to the SNAN sequentially (not in random order as before). The example of corresponding calcium activity in astrocytic layer is shown in Fig. 10B. The dependencies of correlation level of the SNANs cued recalls on different overlapping levels of samples are shown in Fig. 11 for SNAN with astrocytic modulation of synaptic transmission and without it. Results show that including the astrocytic modulation of synaptic transmission into spiking neural network with connections trained according to the Hebbian plasticity leads to a robust improvement of the system retrieval performance for almost all levels of sample overlapping, excluding the highest levels ($> 80\%$). It is important to note that the contribution of astrocytes is especially significant for a high noise value in cue samples (comparing Fig. 11(A) with Fig. 11(B)). On average, in range of samples with overlapping level from 0 to 0.9, the astrocyte-induced enhancements of retrieval quality (in particular, the correlation of cued recalls with ideal samples) amounts to

5% for test samples distorted by 20% noise and 20% for - 30% noise in cue samples. Fig. 11 shows that even for huge pattern overlapping, spurious correlations never dominate in that sense as accuracy of our system is always equal to 100%. Correlation with the target sample always exceeds correlation with the wrong sample.

*6) Comparative analysis:* For comparative analysis, we summarized the performance of the situation-based memory in the developed SNAN and also that of other published studies on the short-term working memory in the SNNs with biologically relevant unsupervised learning rule, such as STDP, in Table S I of the supplementary material. Obviously, our result is one of the best in term of frequency of target pattern activation. The developed SNAN is the only one who can deal with patterns presented to the overlapped neuronal populations, for the best of our knowledge.

To compare our results with the previous studies of the SNN-based classification methods, SNAN is trained and tested on the standard MNIST data set (https://github.com/teavanist/MNIST-JPG) within the proposed situation-based memory framework. The data set used in experiments was partitioned into the training and test sets comprising 10 000 and 2000 samples of 28×28 pixels images of digits 0-9, respectively. Original images from the MNIST data set have been converted into 79×79 patterns to ensure consistency with the size of the pyramidal neuron layer. The SNN was pre-trained on 10 000 training samples distorted by 5% noise applied to the rescaled images with one presentation of the sample. After the SNN pre-training, we trained the SNAN on the initial pool (containing 69 images in total, 3 digits×23 images) using the proposed situation-based learning approach. The MNIST test images presented to the SNAN were corrupted with 20% noise applied to the rescaled images. During the ongoing training-testing process of the situation-based memory in our system in real time, we calculated the correlations between recalls in the SNAN and the images from the MNIST training set. The average accuracy, measured as the proportion of instances when the pattern corresponding to the maximal correlation of SNAN recalls coincided with the target digit, is 97.2 %. This compares favourably with the classification accuracy achieved in the previously reported SNN architectures.

Table S II of the supplementary material summarizes the classification accuracies of the SNN-based systems with biologically plausible learning rules on the MNIST test set. Surprisingly, the pattern recognition system based on SNAN equipped with a simple correlator to process recalls appears to show higher accuracy than all other architectures presented in Table S II of the supplementary material.

Using the procedure described above we also tested how the proposed situation-based memory in the SNAN can deal with the MNIST test set corrupted by correlated noise. A detailed description of these experiments and examples of the noisy test images along with the accuracy attained by the SNAN system in this task are provided in the Supplementary Material. Interestingly, in these additional experiments, the SNAN demonstrated good accuracy on test images distorted with high-level correlated noise without being shown any examples of images corrupted by such noise.

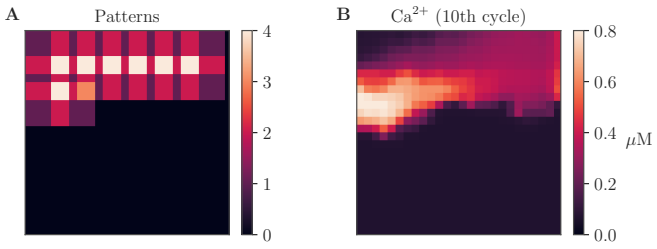


Fig. 10. (A) The example of data set used for evaluation of the impact of the samples overlapping on the SNAN memory performance. The figure shows the case for samples of size $17 \times 17$ pixels with overlapping in 7 pixels which corresponds to overlapping in 41.18 % between the neighboring patterns. (B) The corresponding calcium activity in astrocytic layer.

Comparing the proposed model with recent deep neural network (DNN) models in terms of memory performance can be highly intriguing. However, implementing deep-learning networks using spike-based frameworks is a topic that requires further research [61]. Such an approach is believed to be one of the primary challenges and future prospects of neuromorphic computing. Based on the results obtained thus far, the enrichment of spiking DNN models with astrocytic layers shows great promise. Conducting a comprehensive comparison of performance metrics between spiking DNN models with and without astrocytes would be highly interesting.

*7) Relation to transformer models: Situation-based learning and inference* implemented in the proposed SNAN model are closely related to the idea of *attention*. They also bear functional similarity to popular *transformer* models [12] in that both learning and inference are modulated by contexts inherent to particular situations evolving over time. SNANs' attention mechanism, implemented through astrocytes and relevant signalling pathways, is the consequence of the neuromorphic organisation of the network (cf. [62]). This mechanism enables SNANs to exploit contexts, potentially over large temporal scales, whilst enjoying the benefits of parallel processing of information. The presence of attention circumventing the shortcomings of fixed network topology could explain why SNANs compare favorably to other relevant models, as is shown in Tables S I and S II of the supplementary material.

## VIII. Discussion

The results obtained in the paper could be instrumental for the development of the brain-like (e.g. "strong") artificial intelligence. Inspired by the brain structural and functional organizational hierarchy, neuromorphic hardware systems that implement spike-driven computations could potentially be capable of implementing energy-efficient machine intelligence [61]. In addition, the possibility to enhance learning performance by astrocytes is an important milestone in the ongoing discussion of the role astrocyte-neuronal network interactions in brain processing [16]. Specifically, we have investigated functional roles of different players, e.g. neurons, synapses, plasticity, astrocytes, in the implementation of cognitive information processing tasks in the brain. In particular, it was interesting to observe how the interplay of synaptic changes by

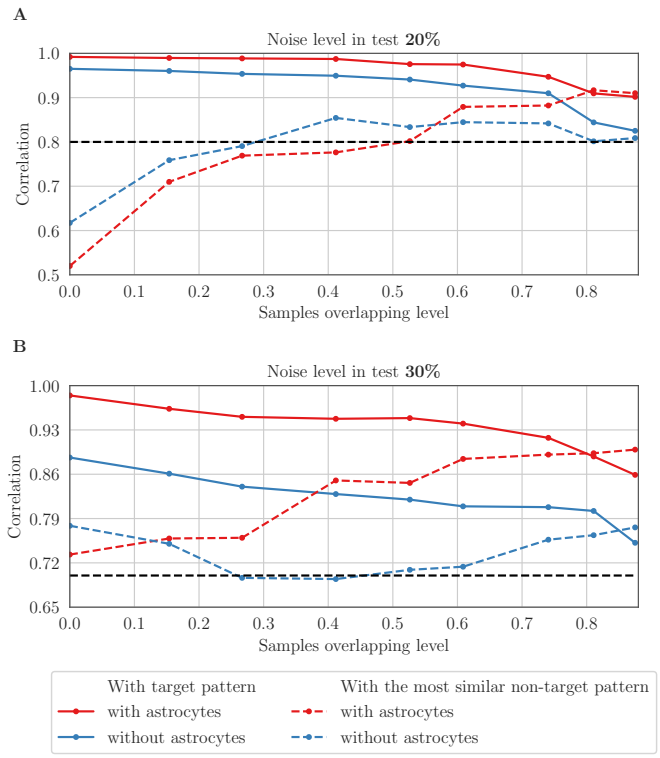


Fig. 11. Impact of the overlapping level in samples on the SNAN memory performance. The dependencies of correlation level of the SNANs cued recalls and samples for different level of sample overlapping are shown for SNAN with astrocytic modulation of synaptic transmission and without it for 20% (A) and 30% (B) noise level. Blue and red dotted lines show correlation of system recalls with the most similar non-target samples. Black dotted lines indicate test patterns correlation.

STDP and by the gliotransmitter modulations improve memory performance (see, for example, Fig. 9).

The STDP-based plasticity represents a key biophysical mechanism of learning in neuronal networks and is considered as one of the most perspective features for SNNs. Modelling and implementing this mechanism involves choosing appropriate values of its parameters. In this work, we did not intend to find optimal parameters of the STDP laws for SNNs as this was beyond the scope of our study. The main focus here was on exploring the holistic interaction between STDP, astrocytes, and neural dynamics in situation-based learning. Nevertheless, we recognise the importance of selecting parameters of STDP-based plasticity appropriately and would therefore like to refer interested readers to relevant literature on the topic [63]–[65].

In memory tasks, the synaptic weights are adjusted following a training protocol by sequential image application. Indeed, we also verified that STDP provided successful in training and information retrieval with certain degree of fidelity. In this context the interneurons balanced network firing by depression and, hence, we can safely assume that they are responsible for lateral inhibition via "selecting" stimulus specific excitation routes. This solely neuronal story can not resolve the problem of "overlapping populations" when different input patterns stimulate similar neuronal groups (up to 50 % of overlaps in our samples). Obviously, the synaptic plasticity alone can not resolve this problem, as it will inevitably lead to false recalls and the decreased performance. However, our research shows that astrocytes can significantly improve this situation.

The astrocytic calcium operates at much slower time scales, hence, the astrocytes can not significantly affect the fast dynamics of neurons and synapses at the time scale of single image processing. Moreover, the calcium excitability has a gradual character [66]. It provides a proportional response to stimuli with different intensities. Thus, the stronger the activation of pyramidal neurons in terms of their discharges intensities over interval of dozen of seconds, the higher the calcium response in the corresponding astrocytes. This way the astrocytes corresponding to the overlapping areas generate larger signals. In turn, they send back different level of modulations during the recall processing. Furthermore, patterns with a high degree of overlap can be successfully resolved, which gives a noticeable increase in the retrieval fidelity.

At functional level, astrocytes supplement neuronal processing by an amplitude modulation in addition to rate encoding by all-or-none firing neurons. At the same time, being distributed in time the astrocytic modulation provides a dynamic separation of overlapping patterns. It is very similar to the reservoir computing in machine learning with traditional artificial neurons [67], [68]. Here, the atrocytes serve as a reservoir naturally "predicting" correct retrieval due to dozen of seconds of stored history.

In general, decoding the physiological meaning of the spatial-temporal $Ca^{2+}$ signalling in astrocytes, its computational properties, and its impact on neuronal signalling remains a major challenge in modern neurobiology [14]. Integration of astrocytic signalling in cognitive processing has implications for understanding the basis of cognitive dysfunction and the development of new therapeutic strategies [16], [69], [70]. SNAN model proposed here could constitute a tool to investigate the role of astrocytes in cognitive functions. To facilitate a stronger link of the proposed SNAN with neuroscience, it might be interesting to employ the mechanisms of intracellular integration of $Ca^{2+}$ signals in astrocytes [38].

Our current work and model do not consider challenges and issues related to the hardware implementation of the model. Having said this, hardware implementation of SNN models is a promising and viable modern trend in the field of neuromorphic electronics. Memristors and memristive electronics can already reproduce *in silico* both spiking neuron dynamics, synaptic signal transmission and synaptic plasticity. With respect to the implementation of astrocytes and the astrocyte-to-neuron control *in silico*, several papers reported successful implementations of the astrocyte dynamics [22], [23], [71]. This suggests that hardware implementations of SNN-based neuromorphic memory could be viable in the near-future.

Finally, we would like to comment on the biological plausibility and model limitations in capturing the behaviour of real brain circuits. By construction, our neuromorphic SNN model imitates morphological constitutions of real brain networks at the macroscopic level. At this macroscopic level, the model demonstrates that involving astrocytes in the processing circuits can lead to significant improvements in memory performance, as compared to neuronal SNNs without astrocytes

(see Tables S I and S II of the supplementary material). The proposed SNAN model reflects experimental data on the structure, connectivity, and neurophysiology of the interaction between neurons and astrocytes in the underlying cortical tissue [14], [16], [19]. As the prototype of the SNAN model, we utilize our previously published biologically plausible computational model of working memory [31]. This model consists of a SNN interacting with a network of astrocytes. In order to enhance its bio-fidelity, we enriched the model with an unsupervised synaptic learning rule based on spike-timing-dependent Hebbian plasticity, as well as a layer of inhibitory neurons [61].

Our biologically relevant, yet still general, modeling approach has ultimately provided insight into the hypothesis of astrocytes participating in memory formation. This hypothesis has emerged from various experimental findings on the contribution of astrocyte signaling to information processing and cognitive function [16], [17]. However, many of these cases lack a comprehensive understanding of the precise mechanisms underlying the astrocytic contribution, making our understanding somewhat fragmented. Therefore, further research is necessary to elucidate the specific role of astrocytic action in memory processes.

It is difficult to compare true human memory with any given and fixed mathematical model as our understanding of memory and its mechanisms is far from complete. Moreover, this understanding is continuously evolving. Circuits of true memory are involved in (and are affected by) many complex biological processes, including hormonal regulations at the micro level, and emotions and stresses at the psychophysiological level. These factors may significantly affect memory performance in different "intrinsic situations", somewhat similar to what we modelled here as "external situations". In this context, by involving astrocytic components, our model offers a framework capable of accounting for factors previously considered exogenous. Remarkably, we show here that doing so is advantageous as compared to other models of memory (see Tables S I and S II of the supplementary material). Further steps could consider including and assessing the performance of brain circuits which are directly responsible for memory function, for example, the hippocampus. The topological organisation of cells in such structures is more complicated than simple layered architectures which are typical artificial neuronal networks including SNNs. The advantage of considering more complicated topologies of networks could be to explore the existence of architectures optimizing network learning and retrieval tasks. Another point which is missed in almost all mathematical models of SNNs is structural plasticity – dynamic changes in the number of connections, neurons, and astrocytes in the network and their properties. Finally, all living networks have an afferentation facilitating ongoing information exchange with the external world, forming processing pathways from the sensory stimuli, e.g. visual images in our case, to execution signals, repository system and others. Including, modelling, and analysing these could be natural steps towards bringing performance of neuromorphic SNNs to that of true living brains.

## IX. Conclusion

This paper presents a novel approach to temporal non-IID data organization for machine learning in spiking neuronal networks. The effectiveness of data formalization in situation-based pools is demonstrated by the short-term memory task implemented by the brain-inspired spiking neuron-astrocytic network (SNAN). The SNAN includes a layer of principle (pyramidal) neurons supplied by a group of inhibitory interneurons. Synaptic connections in the pyramidal layer self-adjust adaptively according to the Hebbian-like spike timing dependent plasticity (STDP). Following morphological brain synaptic organization, the pyramidal neurons are accompanied by astrocytes organized in the the form of a layer network (see Fig. 3). Astrocytic modulation of neuronal activity represents the activity-dependent short-term synaptic plasticity which induces the stimulus-specific local spatial synchronization in neuronal ensembles. The synergistic interplay between fast spiking neuronal network trained on the general data set and slow astrocytic syncytia provides buffering of situation-based data pools by the selective coordination of neuronal signalling, which results in successful storage and retrieval of highly overlapped information patterns. We demonstrated that the astrocyte-induced influence on synaptic transmission results in 10% enhancement of spiking neural network memory performance in terms of correlation level between the cued retrievals and samples for strong 50% overlapped patterns.

## X. Code availability

The code is available at https://github.com/altergot/Neuron-astrocyte-network-Situation-associated-memory.

## Acknowledgments

The reported study was funded in part by Russian Science Foundation Grant No. 22-12-00216 for the model development (Sections 5,7A,7B1-3) and in part by the National Center for Physics and Mathematics (project "Artificial intelligence and big data in technical, industrial, natural and social systems") for the situation-based memory concept development (Sections 4,6,7B4-5). AZ is supported by a Medical Research Council grant (MR/R02524X/1). SG is supported by Russian Science Foundation Grant No. 21-72-10129 (Sections 7B6-7,8). IT is supported by the UKRI Turing AI Acceleration Fellowship (EP/V025295/2).

## References

[1] P. L. Anthony, M.and Bartlett, *Neural network learning: Theoretical foundations*. Cambridge university press, 1999.

[2] V. N. Vapnik, "An overview of statistical learning theory," *IEEE Transactions on Neural Networks*, vol. 10, no. 5, pp. 988–999, 1999.

[3] F. Cucker and S. Smale, "On the mathematical foundations of learning," *Bulletin of the American mathematical society*, vol. 39, no. 1, pp. 1–49, 2002.

[4] A. Bastounis, A. C. Hansen, and V. Vlačić, "The mathematics of adversarial attacks in ai–why deep learning is unstable despite the existence of stable neural networks," *arXiv preprint arXiv:2109.06098*, 2021.

[5] J. Lu, A. Liu, F. Dong, F. Gu, J. Gama, and G. Zhang, "Learning under concept drift: A review," *IEEE transactions on knowledge and data engineering*, vol. 31, no. 12, pp. 2346–2363, 2018.

[6] I. Tyukin, A. N. Gorban, C. Calvo, J. Makarova, and V. A. Makarov, "High-dimensional brain: A tool for encoding and rapid learning of memories by single neurons," *Bulletin of Mathematical Biology*, vol. 81, no. 11, pp. 4856–4888, Mar. 2018. [Online]. Available: https://doi.org/10.1007/s11538-018-0415-5

[7] A. N. Gorban, V. A. Makarov, and I. Y. Tyukin, "The unreasonable effectiveness of small neural ensembles in high-dimensional brain," *Physics of Life Reviews*, vol. 29, pp. 55–88, Jul. 2019. [Online]. Available: https://doi.org/10.1016/j.plrev.2018.09.005

[8] I. Y. Tyukin, A. N. Gorban, M. H. Alkhudaydi, and Q. Zhou, "Demystification of few-shot and one-shot learning," May 2021. [Online]. Available: https://arxiv.org/pdf/2104.12174.pdf

[9] A. N. Gorban, B. Grechuk, E. M. Mirkes, S. V. Stasenko, and I. Y. Tyukin, "High-dimensional separability for one- and few-shot learning," *Entropy*, vol. 23, no. 8, p. 1090, Aug. 2021. [Online]. Available: https://doi.org/10.3390/e23081090

[10] Y. Yufik and R. Malhotra, "Situational understanding in the human and the machine," *Frontiers in Systems Neuroscience*, vol. 15, Dec. 2021. [Online]. Available: https://doi.org/10.3389/fnsys.2021.786252

[11] M. R. Endsley and E. S. Connors, "Foundation and challenges," in *Advances in Information Security*. Springer International Publishing, 2014, pp. 7–27. [Online]. Available: https://doi.org/10.1007/978-3-319-11391-3_2

[12] A. Vaswani, N. Shazeer, N. Parmar, J. Uszkoreit, L. Jones, A. N. Gomez, Ł. Kaiser, and I. Polosukhin, "Attention is all you need," *Advances in neural information processing systems*, vol. 30, 2017.

[13] A. Verkhratsky and M. Nedergaard, "Physiology of astroglia," *Physiological Reviews*, vol. 98, no. 1, pp. 239–389, Jan. 2018. [Online]. Available: https://doi.org/10.1152/physrev.00042.2016

[14] A. Semyanov, C. Henneberger, and A. Agarwal, "Making sense of astrocytic calcium signals — from acquisition to interpretation," *Nature Reviews Neuroscience*, vol. 21, no. 10, pp. 551–564, Sep. 2020. [Online]. Available: https://doi.org/10.1038/s41583-020-0361-8

[15] A. Araque, G. Carmignoto, P. G. Haydon, S. H. Oliet, R. Robitaille, and A. Volterra, "Gliotransmitters travel in time and space," *Neuron*, vol. 81, no. 4, pp. 728–739, Feb. 2014. [Online]. Available: https://doi.org/10.1016/j.neuron.2014.02.007

[16] M. Santello, N. Toni, and A. Volterra, "Astrocyte function from information processing to cognition and cognitive impairment," *Nature Neuroscience*, vol. 22, no. 2, pp. 154–166, Jan. 2019. [Online]. Available: https://doi.org/10.1038/s41593-018-0325-8

[17] J. Nagai, X. Yu, T. Papouin, E. Cheong, M. R. Freeman, K. R. Monk, M. H. Hastings, P. G. Haydon, D. Rowitch, S. Shaham, and B. S. Khakh, "Behaviorally consequential astrocytic regulation of neural circuits," *Neuron*, vol. 109, no. 4, pp. 576–596, Feb. 2021. [Online]. Available: https://doi.org/10.1016/j.neuron.2020.12.008

[18] P. Kofuji and A. Araque, "Astrocytes and behavior," *Annual Review of Neuroscience*, vol. 44, no. 1, pp. 49–67, Jul. 2021. [Online]. Available: https://doi.org/10.1146/annurev-neuro-101920-112225

[19] K. V. Kastanenka, R. Moreno-Bote, M. D. Pittà, G. Perea, A. Eraso-Pichot, R. Masgrau, K. E. Poskanzer, and E. Galea, "A roadmap to integrate astrocytes into systems neuroscience," *Glia*, vol. 68, no. 1, pp. 5–26, May 2019. [Online]. Available: https://doi.org/10.1002/glia.23632

[20] J. Liu, L. J. Mcdaid, J. Harkin, S. Karim, A. P. Johnson, A. G. Millard, J. Hilder, D. M. Halliday, A. M. Tyrrell, and J. Timmis, "Exploring self-repair in a coupled spiking astrocyte neural network," *IEEE Transactions on Neural Networks and Learning Systems*, vol. 30, no. 3, pp. 865–875, Mar. 2019. [Online]. Available: https://doi.org/10.1109/tnnls.2018.2854291

[21] S. Nazari, M. Amiri, K. Faez, and M. M. V. Hulle, "Information transmitted from bioinspired neuron–astrocyte network improves cortical spiking network's pattern recognition performance," *IEEE Transactions on Neural Networks and Learning Systems*, vol. 31, no. 2, pp. 464–474, Feb. 2020. [Online]. Available: https://doi.org/10.1109/tnnls.2019.2905003

[22] H. Soleimani, M. Bavandpour, A. Ahmadi, and D. Abbott, "Digital implementation of a biological astrocyte model and its application," *IEEE Transactions on Neural Networks and Learning Systems*, vol. 26, no. 1, pp. 127–139, Jan. 2015. [Online]. Available: https://doi.org/10.1109/tnnls.2014.2311839

[23] S. Nazari, K. Faez, M. Amiri, and E. Karami, "A digital implementation of neuron–astrocyte interaction for neuromorphic applications," *Neural Networks*, vol. 66, pp. 79–90, Jun. 2015. [Online]. Available: https://doi.org/10.1016/j.neunet.2015.01.005

[24] M. Hayati, M. Nouri, S. Haghiri, and D. Abbott, "A digital realization of astrocyte and neural glial interactions," *IEEE Transactions on Biomedical Circuits and Systems*, vol. 10, no. 2, pp. 518–529, Apr. 2016. [Online]. Available: https://doi.org/10.1109/tbcas.2015.2450837

[25] S. Y. Gordleeva, S. A. Lebedev, M. A. Rumyantseva, and V. B. Kazantsev, "Astrocyte as a detector of synchronous events of a neural network," *JETP Letters*, vol. 107, no. 7, pp. 440–445, Apr. 2018. [Online]. Available: https://doi.org/10.1134/s0021364018070032

[26] E. V. Pankratova, A. I. Kalyakulina, S. V. Stasenko, S. Y. Gordleeva, I. A. Lazarevich, and V. B. Kazantsev, "Neuronal synchronization enhanced by neuron–astrocyte interaction," *Nonlinear Dynamics*, vol. 97, no. 1, pp. 647–662, May 2019. [Online]. Available: https://doi.org/10.1007/s11071-019-05004-7

[27] S. Makovkin, E. Kozinov, M. Ivanchenko, and S. Gordleeva, "Controlling synchronization of gamma oscillations by astrocytic modulation in a model hippocampal neural network," *Scientific Reports*, vol. 12, no. 1, Apr. 2022. [Online]. Available: https://doi.org/10.1038/s41598-022-10649-3

[28] O. Kanakov, S. Gordleeva, A. Ermolaeva, S. Jalan, and A. Zaikin, "Astrocyte-induced positive integrated information in neuron-astrocyte ensembles," *Physical Review E*, vol. 99, no. 1, Jan. 2019. [Online]. Available: https://doi.org/10.1103/physreve.99.012418

[29] O. Kanakov, S. Gordleeva, and A. Zaikin, "Integrated information in the spiking–bursting stochastic model," *Entropy*, vol. 22, no. 12, p. 1334, Nov. 2020. [Online]. Available: https://doi.org/10.3390/e22121334

[30] L. Abrego, S. Gordleeva, O. Kanakov, M. Krivonosov, and A. Zaikin, "Estimating integrated information in bidirectional neuron-astrocyte communication," *Physical Review E*, vol. 103, no. 2, Feb. 2021. [Online]. Available: https://doi.org/10.1103/physreve.103.022410

[31] S. Y. Gordleeva, Y. A. Tsybina, M. I. Krivonosov, M. V. Ivanchenko, A. A. Zaikin, V. B. Kazantsev, and A. N. Gorban, "Modeling working memory in a spiking neuron network accompanied by astrocytes," *Frontiers in Cellular Neuroscience*, vol. 15, Mar. 2021. [Online]. Available: https://doi.org/10.3389/fncel.2021.631485

[32] S. Y. Gordleeva, Y. A. Lotareva, M. I. Krivonosov, A. A. Zaikin, M. V. Ivanchenko, and A. N. Gorban, "Astrocytes organize associative memory," in *Advances in Neural Computation, Machine Learning, and Cognitive Research III*. Springer International Publishing, Sep. 2019, pp. 384–391.

[33] A. Zhao, A. Ermolaeva, E. Ullner, J. Kurths, S. Gordleeva, and A. Zaikin, "Noise-induced artificial intelligence," *PHYSICAL REVIEW RESEARCH*, vol. 4, no. 043069, Oct. 2022. [Online]. Available: https://journals.aps.org/prresearch/pdf/10.1103/PhysRevResearch.4.043069

[34] M. D. Pittà and N. Brunel, "Multiple forms of working memory emerge from synapse–astrocyte interactions in a neuron–glia network model," *Proceedings of the National Academy of Sciences*, vol. 119, no. 43, Oct. 2022. [Online]. Available: https://doi.org/10.1073/pnas.2207912119

[35] S. Becker, A. Nold, and T. Tchumatchenko, "Modulation of working memory duration by synaptic and astrocytic mechanisms," *PLOS Computational Biology*, vol. 18, no. 10, p. e1010543, Oct. 2022. [Online]. Available: https://doi.org/10.1371/journal.pcbi.1010543

[36] Y. Tsybina, I. Kastalskiy, M. Krivonosov, A. Zaikin, V. Kazantsev, A. N. Gorban, and S. Gordleeva, "Astrocytes mediate analogous memory in a multi-layer neuron–astrocyte network," *Neural Computing and Applications*, Feb. 2022. [Online]. Available: https://doi.org/10.1007/s00521-022-06936-9

[37] S. Y. Makovkin, I. V. Shkerin, S. Y. Gordleeva, and M. V. Ivanchenko, "Astrocyte-induced intermittent synchronization of neurons in a minimal network," *Chaos, Solitons & Fractals*, vol. 138, p. 109951, Sep. 2020. [Online]. Available: https://doi.org/10.1016/j.chaos.2020.109951

[38] S. Y. Gordleeva, A. V. Ermolaeva, I. A. Kastalskiy, and V. B. Kazantsev, "Astrocyte as spatiotemporal integrating detector of neuronal activity," *Frontiers in Physiology*, vol. 10, Apr. 2019. [Online]. Available: https://doi.org/10.3389/fphys.2019.00294

[39] A. Hodgkin and A. Huxley, "A quantitative description of membrane current and its application to conduction and excitation in nerve," *Bulletin of Mathematical Biology*, vol. 52, no. 1-2, pp. 25–71, 1990. [Online]. Available: https://doi.org/10.1016/s0092-8240(05)80004-7

[40] Y. Zhang, Y. Xu, Z. Yao, and J. Ma, "A feasible neuron for estimating the magnetic field effect," *Nonlinear Dynamics*, vol. 102, no. 3, pp. 1849–1867, Oct. 2020. [Online]. Available: https://doi.org/10.1007/s11071-020-05991-y

[41] C. Morris and H. Lecar, "Voltage oscillations in the barnacle giant muscle fiber," *Biophysical Journal*, vol. 35, no. 1, pp. 193–213, Jul. 1981. [Online]. Available: https://doi.org/10.1016/s0006-3495(81)84782-0

[42] Y. Xu, M. Liu, Z. Zhu, and J. Ma, "Dynamics and coherence resonance in a thermosensitive neuron driven by photocurrent," *Chinese*

*Physics B*, vol. 29, no. 9, p. 098704, Aug. 2020. [Online]. Available: https://doi.org/10.1088/1674-1056/ab9dee

[43] E. Izhikevich, "Simple model of spiking neurons," *IEEE Transactions on Neural Networks*, vol. 14, no. 6, pp. 1569–1572, Nov. 2003. [Online]. Available: https://doi.org/10.1109/tnn.2003.820440

[44] V. B. Kazantsev and S. Y. Asatryan, "Bistability induces episodic spike communication by inhibitory neurons in neuronal networks," *Physical Review E*, vol. 84, no. 3, Sep. 2011. [Online]. Available: https://doi.org/10.1103/physreve.84.031913

[45] P. M. Esir, S. Y. Gordleeva, A. Y. Simonov, A. N. Pisarchik, and V. B. Kazantsev, "Conduction delays can enhance formation of up and down states in spiking neuronal networks," *Physical Review E*, vol. 98, no. 5, Nov. 2018. [Online]. Available: https://doi.org/10.1103/physreve.98.052401

[46] M. M. Halassa, T. Fellin, H. Takano, J.-H. Dong, and P. G. Haydon, "Synaptic islands defined by the territory of a single astrocyte," *Journal of Neuroscience*, vol. 27, no. 24, pp. 6473–6477, Jun. 2007. [Online]. Available: https://doi.org/10.1523/jneurosci.1419-07.2007

[47] G. Ullah, P. Jung, and A. Cornell-Bell, "Anti-phase calcium oscillations in astrocytes via inositol (1, 4, 5)-trisphosphate regeneration," *Cell Calcium*, vol. 39, no. 3, pp. 197–208, Mar. 2006. [Online]. Available: https://doi.org/10.1016/j.ceca.2005.10.009

[48] T. Yamamoto, A. Ochalski, E. L. Hertzberg, and J. I. Nagy, "On the organization of astrocytic gap junctions in rat brain as suggested by LM and EM immunohistochemistry of connexin43 expression," *The Journal of Comparative Neurology*, vol. 302, no. 4, pp. 853–883, Dec. 1990. [Online]. Available: https://doi.org/10.1002/cne.903020414

[49] J. I. Nagy and J. E. Rash, "Connexins and gap junctions of astrocytes and oligodendrocytes in the CNS," *Brain Research Reviews*, vol. 32, no. 1, pp. 29–44, Mar. 2000. [Online]. Available: https://doi.org/10.1016/s0165-0173(99)00066-1

[50] S. Y. Gordleeva, S. V. Stasenko, A. V. Semyanov, A. E. Dityatev, and V. B. Kazantsev, "Bi-directional astrocytic regulation of neuronal activity within a network," *Frontiers in Computational Neuroscience*, vol. 6, 2012. [Online]. Available: https://doi.org/10.3389/fncom.2012.00092

[51] T. Fellin, O. Pascual, S. Gobbo, T. Pozzan, P. G. Haydon, and G. Carmignoto, "Neuronal synchrony mediated by astrocytic glutamate through activation of extrasynaptic NMDA receptors," *Neuron*, vol. 43, no. 5, pp. 729–743, Sep. 2004. [Online]. Available: https://doi.org/10.1016/j.neuron.2004.08.011

[52] N. Chen, H. Sugihara, J. Sharma, G. Perea, J. Petravicz, C. Le, and M. Sur, "Nucleus basalis-enabled stimulus-specific plasticity in the visual cortex is mediated by astrocytes," *Proceedings of the National Academy of Sciences*, vol. 109, no. 41, pp. E2832–E2841, Sep. 2012. [Online]. Available: https://doi.org/10.1073/pnas.1206557109

[53] G. Perea and A. Araque, "Astrocytes potentiate transmitter release at single hippocampal synapses," *Science*, vol. 317, no. 5841, pp. 1083–1086, Aug. 2007. [Online]. Available: https://doi.org/10.1126/science.1144640

[54] M. Navarrete and A. Araque, "Endocannabinoids mediate neuron-astrocyte communication," *Neuron*, vol. 57, no. 6, pp. 883–893, Mar. 2008. [Online]. Available: https://doi.org/10.1016/j.neuron.2008.01.029

[55] ——, "Endocannabinoids potentiate synaptic transmission through stimulation of astrocytes," *Neuron*, vol. 68, no. 1, pp. 113–126, Oct. 2010. [Online]. Available: https://doi.org/10.1016/j.neuron.2010.08.043

[56] A. Mazzoni, S. Panzeri, N. K. Logothetis, and N. Brunel, "Encoding of naturalistic stimuli by local field potential spectra in networks of excitatory and inhibitory neurons," *PLoS Computational Biology*, vol. 4, no. 12, p. e1000239, Dec. 2008. [Online]. Available: https://doi.org/10.1371/journal.pcbi.1000239

[57] M. Chalk, P. Masset, S. Deneve, and B. Gutkin, "Sensory noise predicts divisive reshaping of receptive fields," *PLOS Computational Biology*, vol. 13, no. 6, p. e1005582, Jun. 2017. [Online]. Available: https://doi.org/10.1371/journal.pcbi.1005582

[58] S. Lobov, M. Zhuravlev, V. Makarov, and V. Kazantsev, "Noise enhanced signaling in STDP driven spiking-neuron network," *Mathematical Modelling of Natural Phenomena*, vol. 12, no. 4, pp. 109–124, 2017. [Online]. Available: https://doi.org/10.1051/mmnp/201712409

[59] H. Noh, T. You, J. Mun, and B. Han, "Regularizing deep neural networks by noise: Its interpretation and optimization," *Advances in Neural Information Processing Systems*, vol. 30, 2017.

[60] I. Surazhevsky, V. Demin, A. Ilyasov, A. Emelyanov, K. Nikiruy, V. Rylkov, S. Shchanikov, I. Bordanov, S. Gerasimova, D. Guseinov, N. Malekhonova, D. Pavlov, A. Belov, A. Mikhaylov, V. Kazantsev, D. Valenti, B. Spagnolo, and M. Kovalchuk, "Noise-assisted persistence and recovery of memory state in a memristive spiking neuromorphic network," *Chaos, Solitons & Fractals*, vol. 146, p. 110890, May 2021. [Online]. Available: https://doi.org/10.1016/j.chaos.2021.110890

[61] K. Roy, A. Jaiswal, and P. Panda, "Towards spike-based machine intelligence with neuromorphic computing," *Nature*, vol. 575, no. 7784, pp. 607–617, Nov. 2019. [Online]. Available: https://doi.org/10.1038/s41586-019-1677-2

[62] J. C. Whittington, J. Warren, and T. E. Behrens, "Relating transformers to models and neural representations of the hippocampal formation," *arXiv preprint arXiv:2112.04035*, 2021.

[63] V. Demin, D. Nekhaev, I. Surazhevsky, K. Nikiruy, A. Emelyanov, S. Nikolaev, V. Rylkov, and M. Kovalchuk, "Necessary conditions for STDP-based pattern recognition learning in a memristive spiking neural network," *Neural Networks*, vol. 134, pp. 64–75, Feb. 2021. [Online]. Available: https://doi.org/10.1016/j.neunet.2020.11.005

[64] Z. Wang, S. Joshi, S. Savel'ev, W. Song, R. Midya, Y. Li, M. Rao, P. Yan, S. Asapu, Y. Zhuo, H. Jiang, P. Lin, C. Li, J. H. Yoon, N. K. Upadhyay, J. Zhang, M. Hu, J. P. Strachan, M. Barnell, Q. Wu, H. Wu, R. S. Williams, Q. Xia, and J. J. Yang, "Fully memristive neural networks for pattern classification with unsupervised learning," *Nature Electronics*, vol. 1, no. 2, pp. 137–145, Feb. 2018. [Online]. Available: https://doi.org/10.1038/s41928-018-0023-2

[65] D. Querlioz, O. Bichler, P. Dollfus, and C. Gamrat, "Immunity to device variations in a spiking neural network with memristive nanodevices," *IEEE Transactions on Nanotechnology*, vol. 12, no. 3, pp. 288–295, May 2013. [Online]. Available: https://doi.org/10.1109/tnano.2013.2250995

[66] V. Matrosov, S. Gordleeva, N. Boldyreva, E. Ben-Jacob, V. Kazantsev, and M. D. Pittà, "Emergence of regular and complex calcium oscillations by inositol 1, 4, 5-trisphosphate signaling in astrocytes," in *Springer Series in Computational Neuroscience*. Springer International Publishing, 2019, pp. 151–176. [Online]. Available: https://doi.org/10.1007/978-3-030-00817-8_6

[67] M. Lukoševičius and H. Jaeger, "Reservoir computing approaches to recurrent neural network training," *Computer Science Review*, vol. 3, no. 3, pp. 127–149, Aug. 2009. [Online]. Available: https://doi.org/10.1016/j.cosrev.2009.03.005

[68] P. Vlachas, J. Pathak, B. Hunt, T. Sapsis, M. Girvan, E. Ott, and P. Koumoutsakos, "Backpropagation algorithms and reservoir computing in recurrent neural networks for the forecasting of complex spatiotemporal dynamics," *Neural Networks*, vol. 126, pp. 191–217, Jun. 2020. [Online]. Available: https://doi.org/10.1016/j.neunet.2020.02.016

[69] S. Gordleeva, O. Kanakov, M. Ivanchenko, A. Zaikin, and C. Franceschi, "Brain aging and garbage cleaning," *Seminars in Immunopathology*, vol. 42, no. 5, pp. 647–665, Oct. 2020. [Online]. Available: https://doi.org/10.1007/s00281-020-00816-x

[70] H. J. Whitwell, M. G. Bacalini, O. Blyuss, S. Chen, P. Garagnani, S. Y. Gordleeva, S. Jalan, M. Ivanchenko, O. Kanakov, V. Kustikova, I. P. Mariño, I. Meyerov, E. Ullner, C. Franceschi, and A. Zaikin, "The human body as a super network: Digital methods to analyze the propagation of aging," *Frontiers in Aging Neuroscience*, vol. 12, May 2020. [Online]. Available: https://doi.org/10.3389/fnagi.2020.00136

[71] F. Azad, M. Shalchian, and M. Amiri, "Circuit modelling of 2-AG indirect pathway via astrocyte as a catalyst for synaptic self repair," *Analog Integrated Circuits and Signal Processing*, vol. 95, no. 1, pp. 127–139, Jan. 2018. [Online]. Available: https://doi.org/10.1007/s10470-018-1106-8